Supporting Information for

Selective Sensing of Peroxynitrite by Hf-Based UiO-66-B(OH)$_2$ Metal-Organic Framework: Applicability to Cell Imaging

Mostakim SK,[¥] Soutick Nandi,[¥] Rakesh Kumar Singh, Vishal Trivedi,[‡] and Shyam Biswas*[¥]

[¥] Department of Chemistry, Indian Institute of Technology Guwahati, Guwahati, 781039 Assam, India

[‡] Malaria Research Group, Department of Biosciences and Bioengineering, Indian Institute of Technology Guwahati, 781039 Assam, India

*To whom correspondence should be addressed. E-mail: sbiswas@iitg.ernet.in; Tel: 91-3612583309

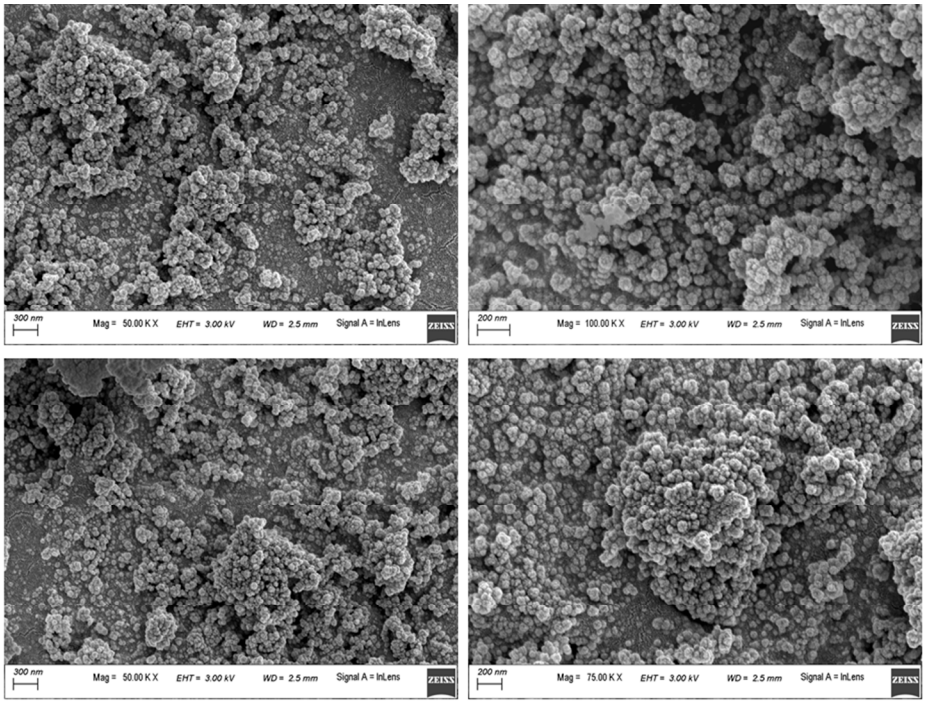

Figure S1. FE-SEM images of **1′**.

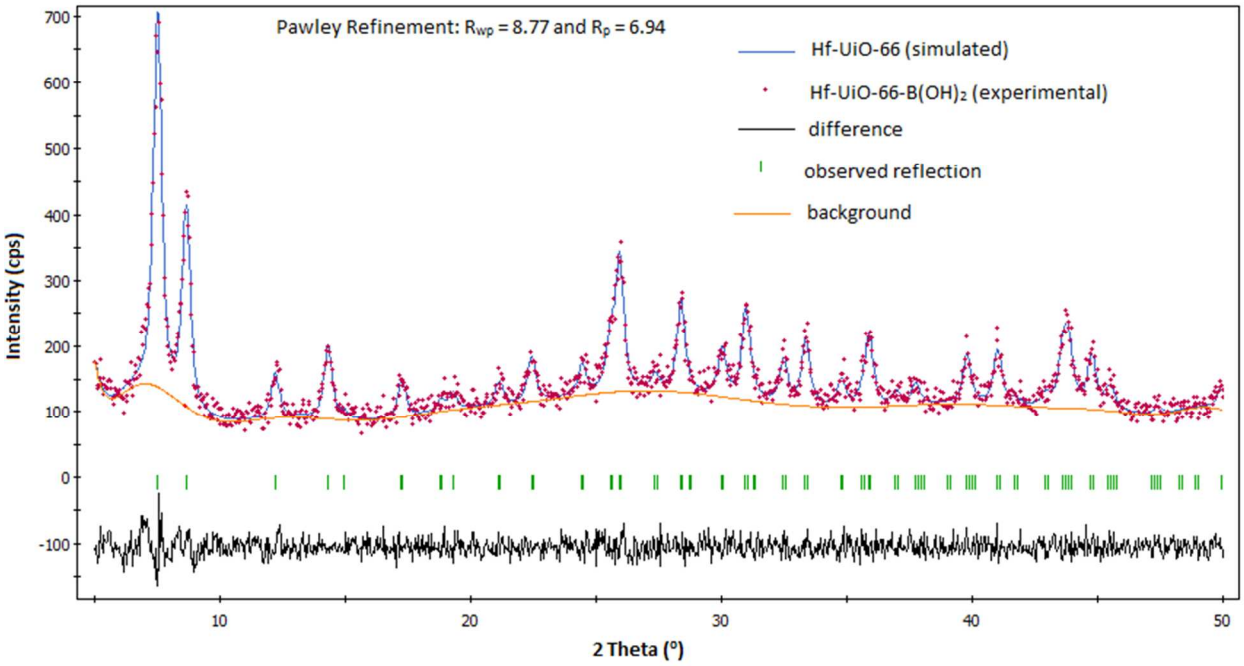

Figure S2. Pawley refinement for the XRPD pattern of as-synthesized **1**. Red dots and blue lines denote observed and calculated patterns, respectively. The peak positions and difference plot are displayed at the bottom (R_p = 6.94, R_{wp} = 8.77).

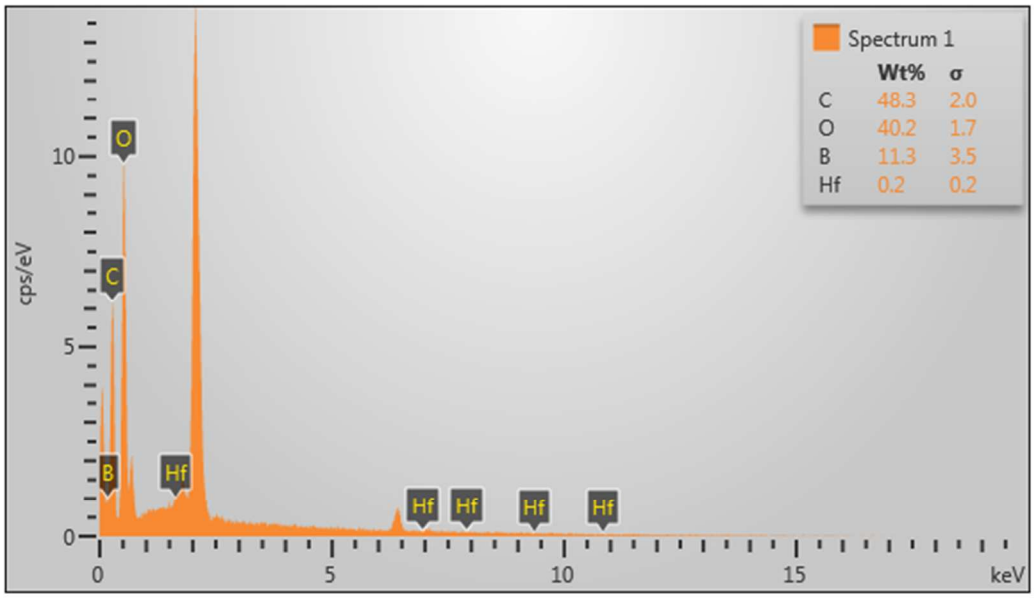

Figure S3. EDX spectrum of **1′**.

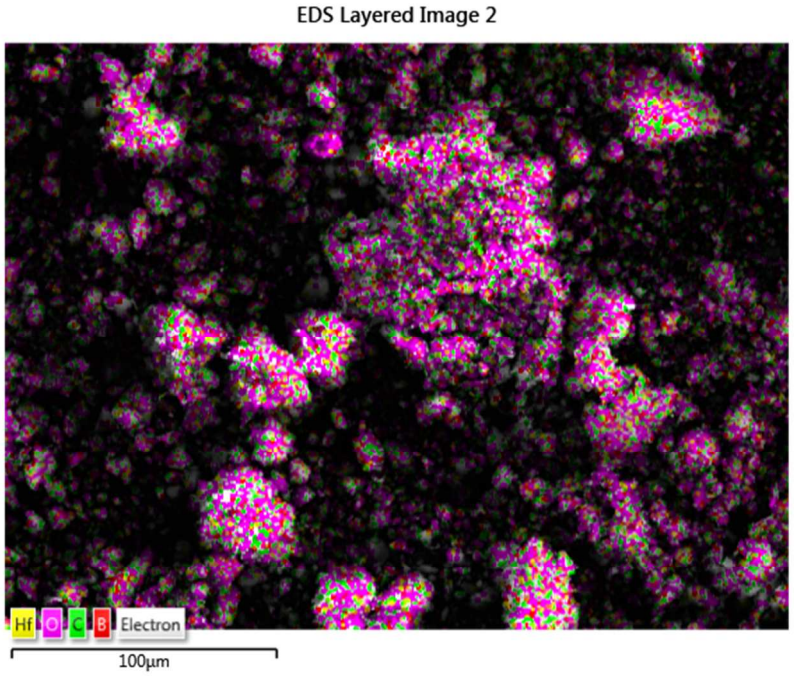

Figure S4. EDX elemental mapping images of **1′**.

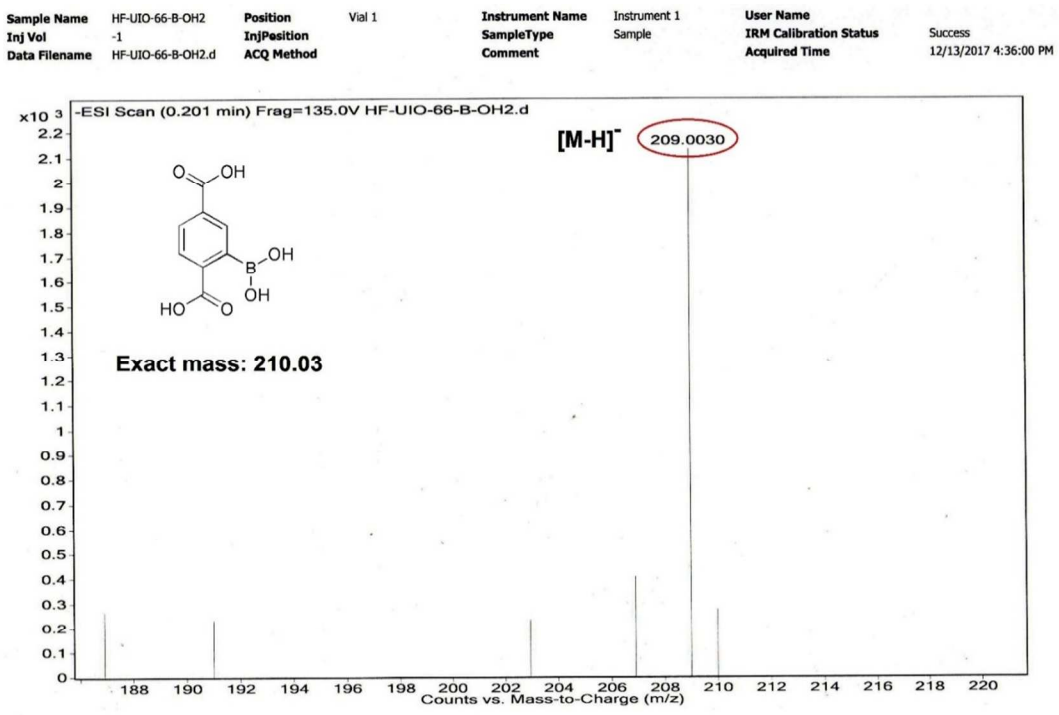

Figure S5. Mass spectrum of **1′** after digestion in HF/MeOH.

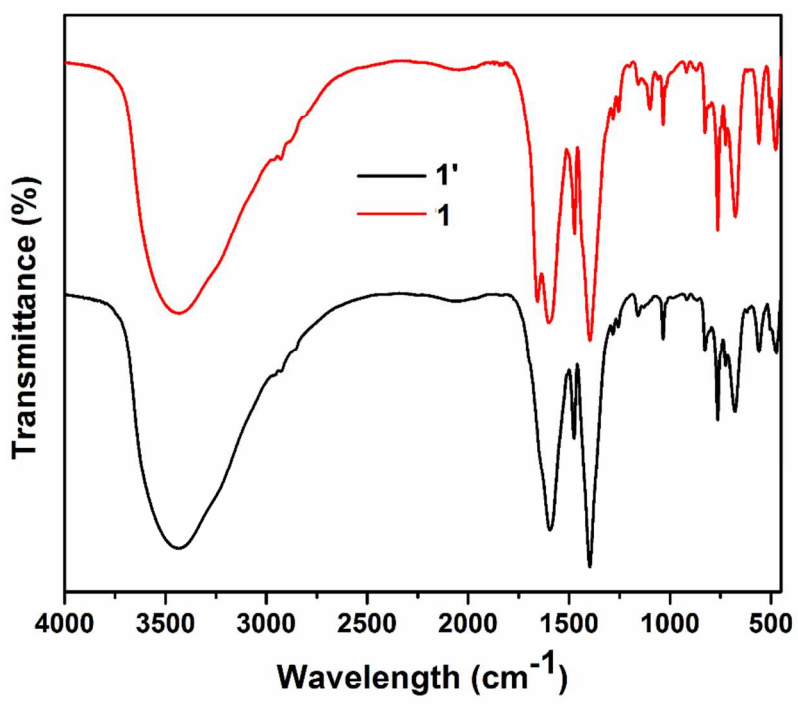

Figure S6. FT-IR spectra of as-synthesized **1** (red) and activated **1′** (black).

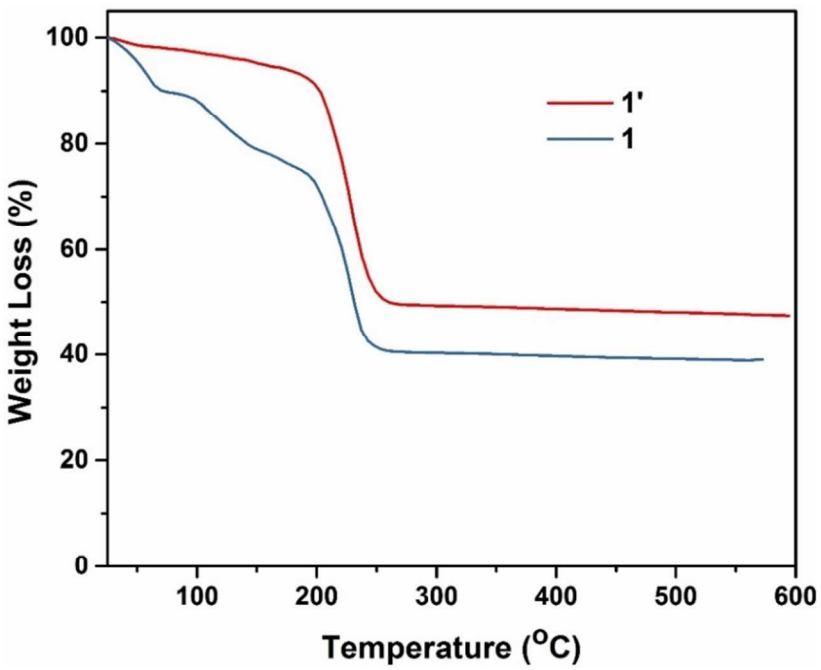

Figure S7. TG curves of as-synthesized (blue) and activated (red) forms of **1** measured under air atmosphere with a heating rate of 5 °C min^{-1}.

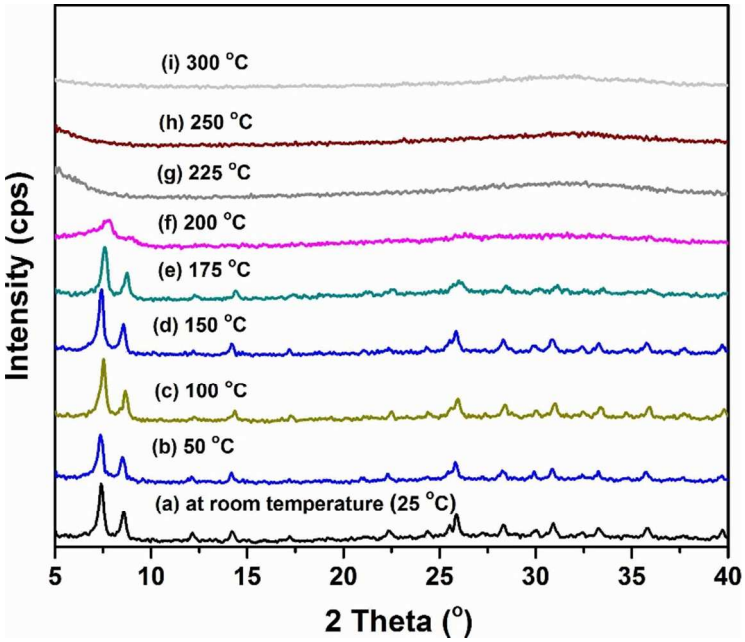

Figure S8. Temperature-dependent XRPD patterns of the activated Hf-UiO-66-$B(OH)_2$ MOF.

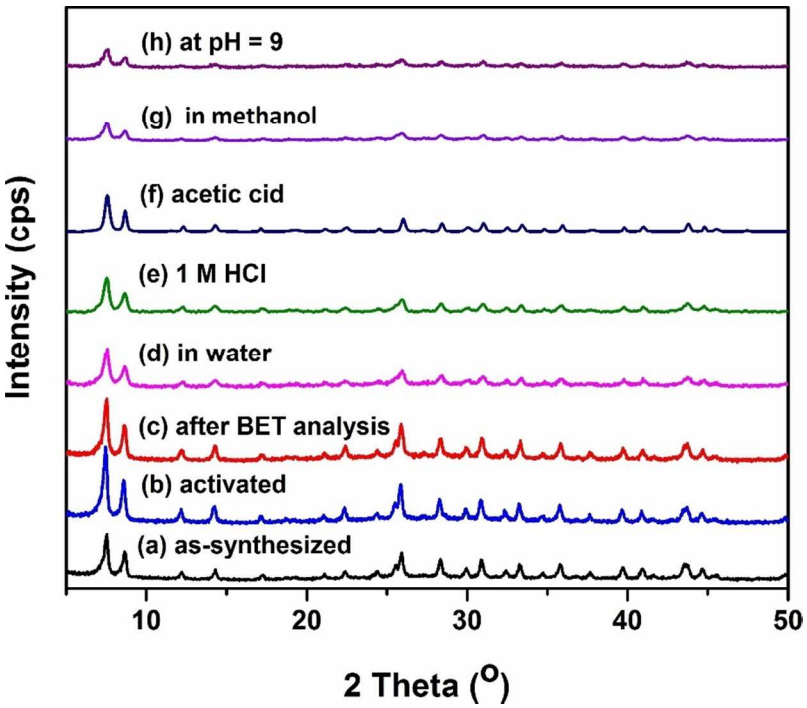

Figure S9. XRPD patterns of **1′** in different forms: as-synthesized (a); activated (b); after BET measurement (c); after treatment with water (d); after treatment with 1(M) HCl (e); after treatment with acetic acid (f); after treatment with methanol (g); after treatment with NaOH at pH = 9 (h).

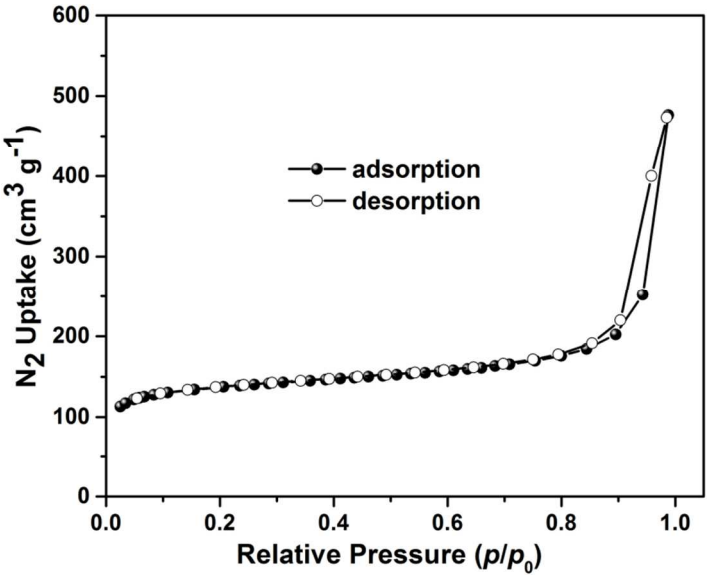

Figure S10. N_2 adsorption (filled circles) and desorption (empty circles) isotherms of **1′** measured at –196 °C.

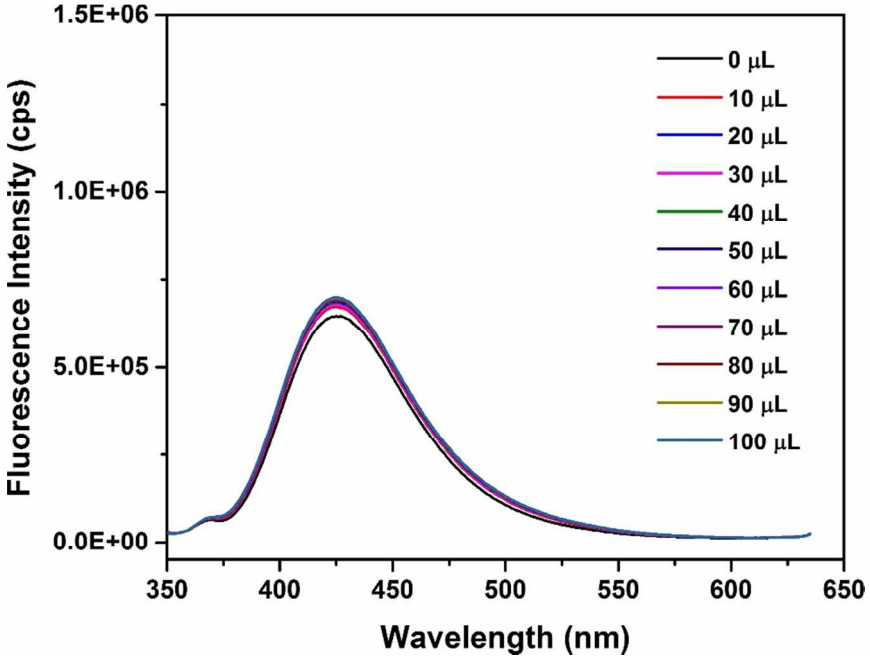

Figure S11. Fluorescence response of **1′** towards 0.5 mM ^{t}BuO$^{\bullet}$ (λ_{ex} = 330 nm and λ_{em} = 426 nm).

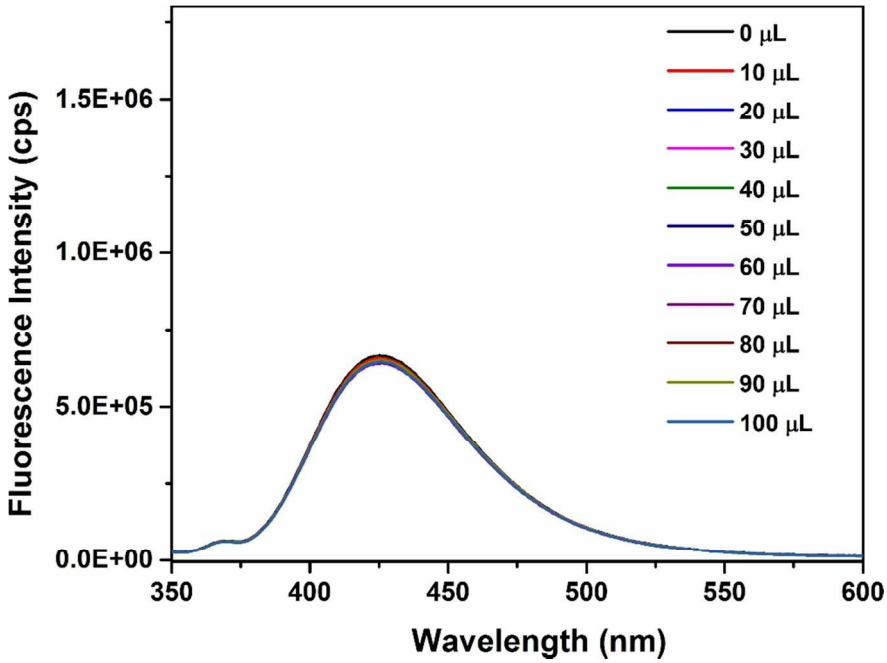

Figure S12. Fluorescence response of **1′** towards 0.5 mM NaOCl (λ_{ex} = 330 nm and λ_{em} = 426 nm).

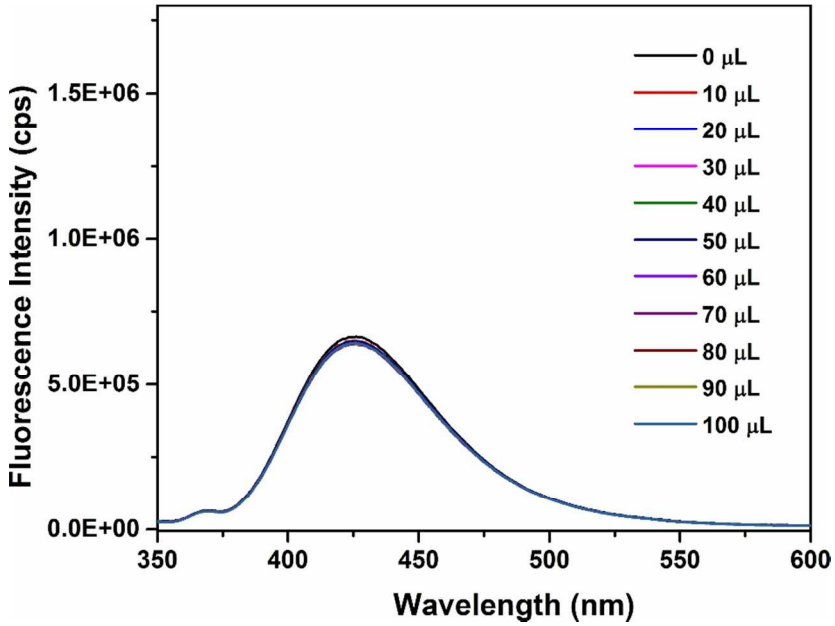

Figure S13. Fluorescence response of **1'** towards 0.5 mM TBHP (λ_{ex} = 330 nm and λ_{em} = 426 nm).

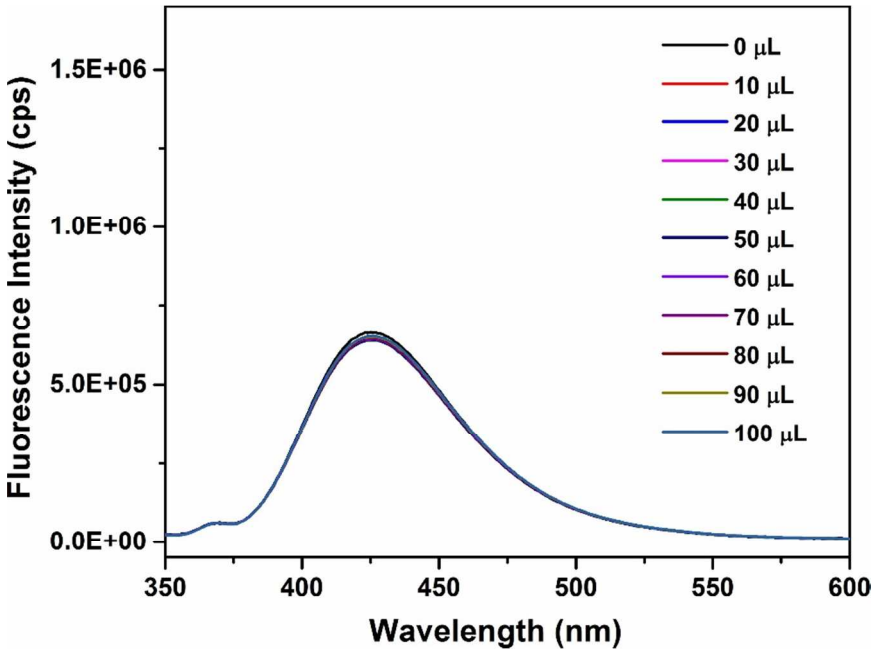

Figure S14. Fluorescence response of **1′** towards 0.5 mM $O_2^{\bullet-}$ (λ_{ex} = 330 nm and λ_{em} = 426 nm).

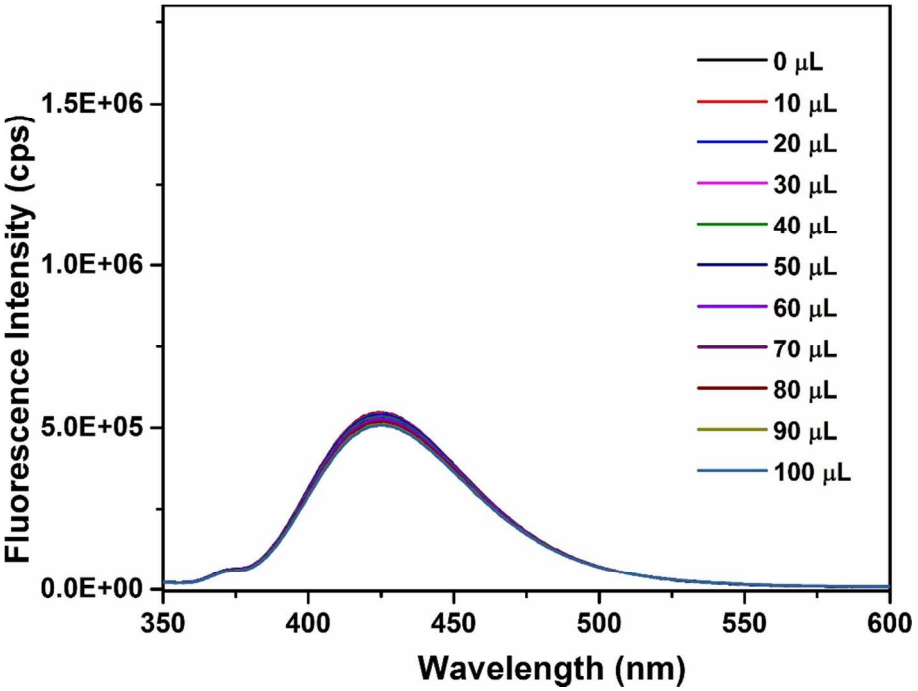

Figure S15. Fluorescence response of **1′** towards 0.5 mM $HO^{\bullet}$ (λ_{ex} = 330 nm and λ_{em} = 426 nm).

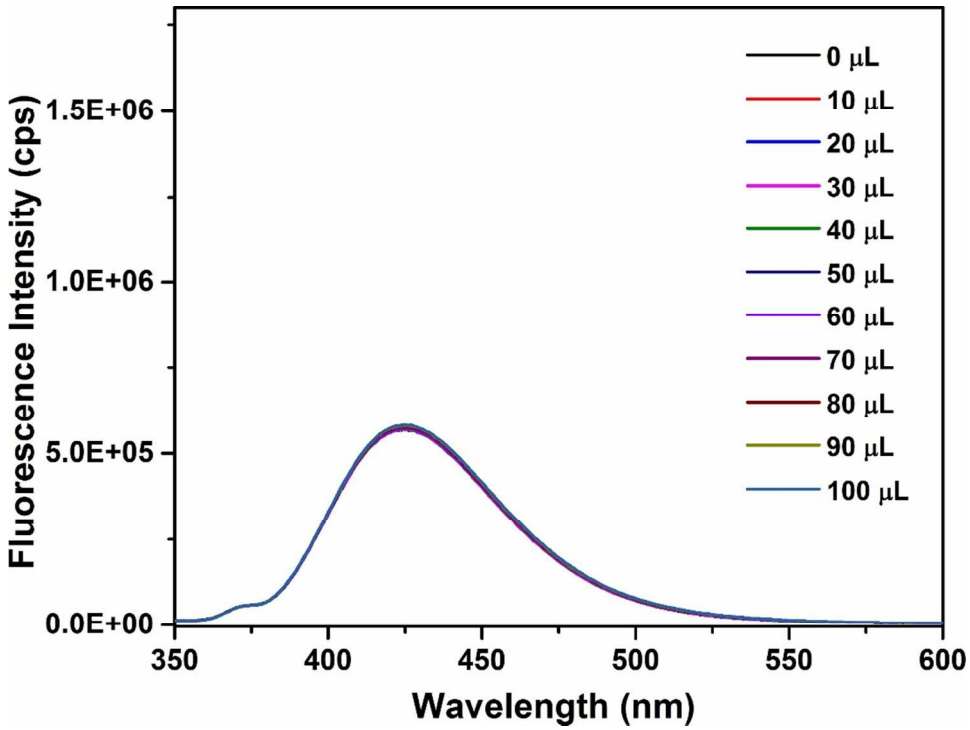

Figure S16. Fluorescence response of **1′** towards 0.5 mM $^1O_2$ (λ_{ex} = 330 nm and λ_{em} = 426 nm).

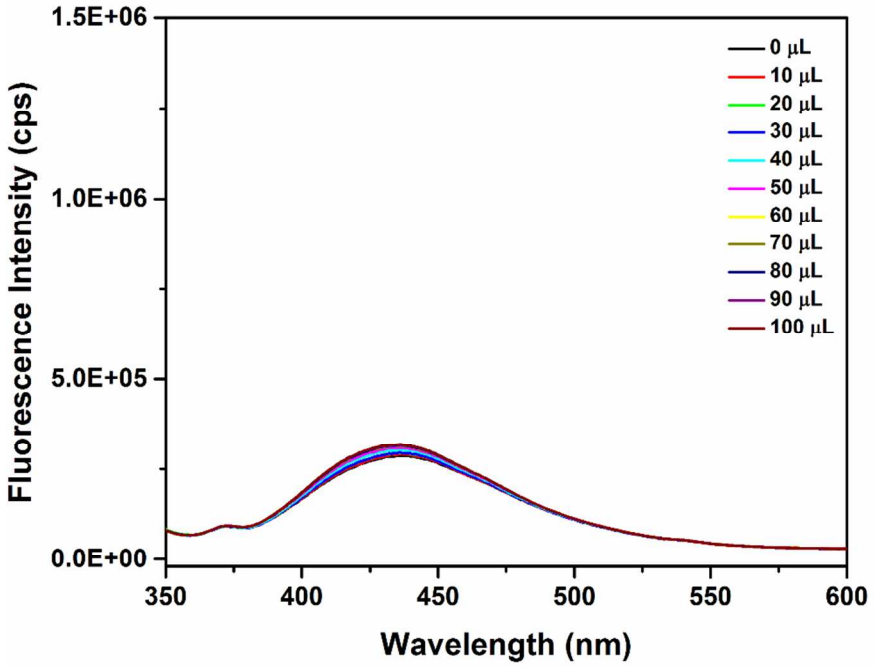

Figure S17. Fluorescence response of **1′** towards 0.5 mM NO$^{\bullet}$ (λ_{ex} = 330 nm and λ_{em} = 426 nm).

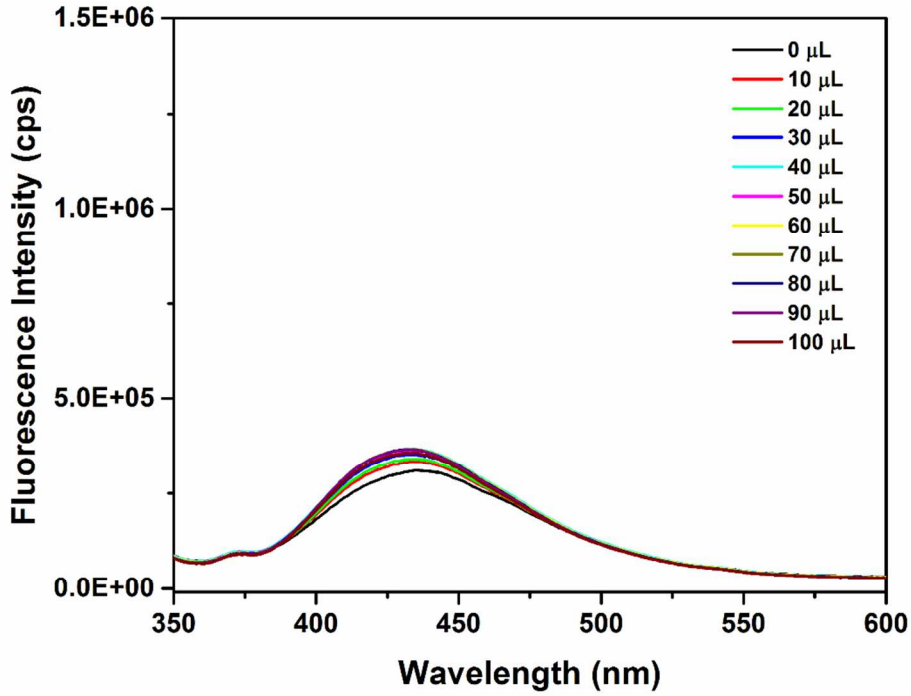

Figure S18. Fluorescence response of **1′** towards 0.5 mM NO^+ (λ_{ex} = 330 nm and λ_{em} = 426 nm).

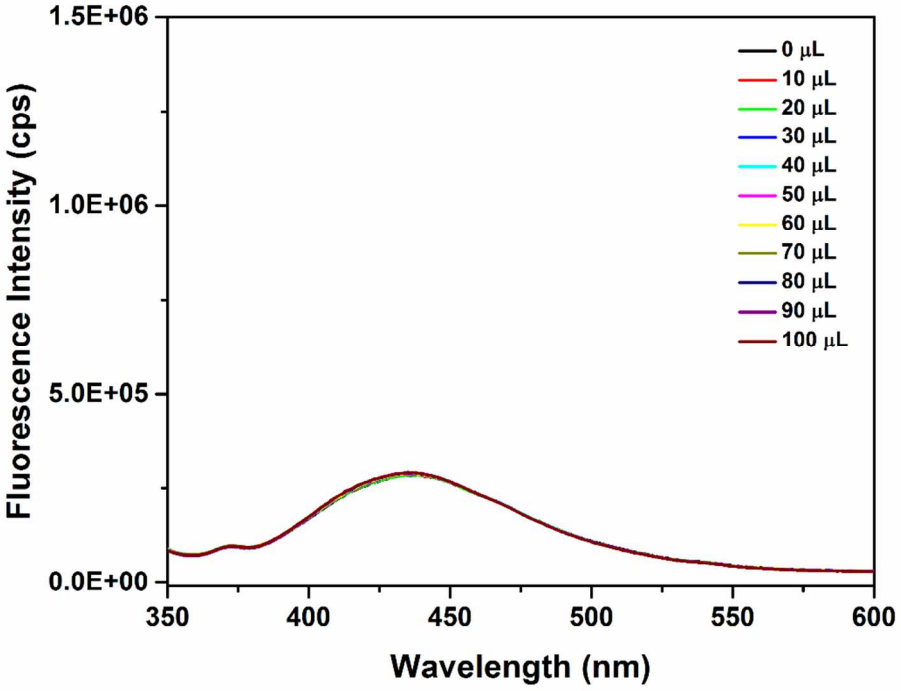

Figure S19. Fluorescence response of **1′** towards 0.5 mM NO_2^- (λ_{ex} = 330 nm and λ_{em} = 426 nm).

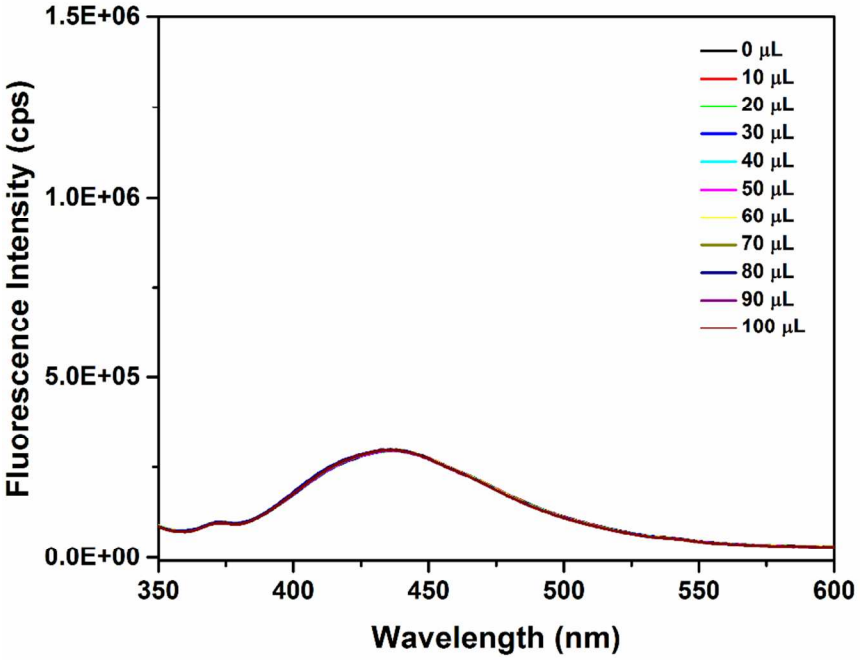

Figure S20. Fluorescence response of **1′** towards 0.5 mM NO_3^- (λ_{ex} = 330 nm and λ_{em} = 426 nm).

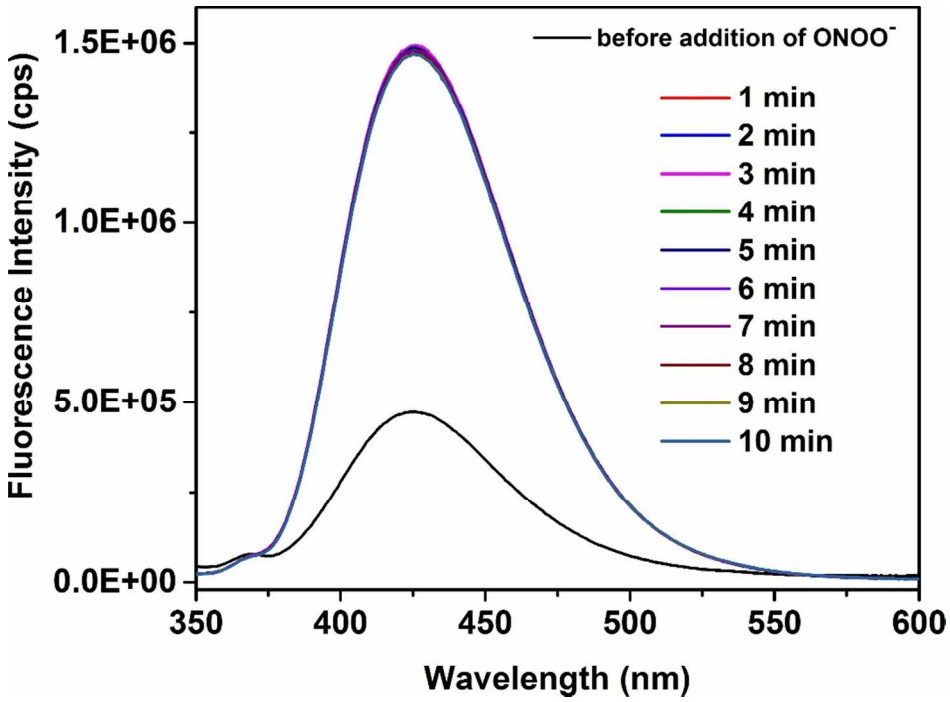

Figure S21. Change in the fluorescence spectrum of **1′** in presence of 0.5 mM $ONOO^-$ as a function of time (λ_{ex} = 330 nm and λ_{em} = 426 nm).

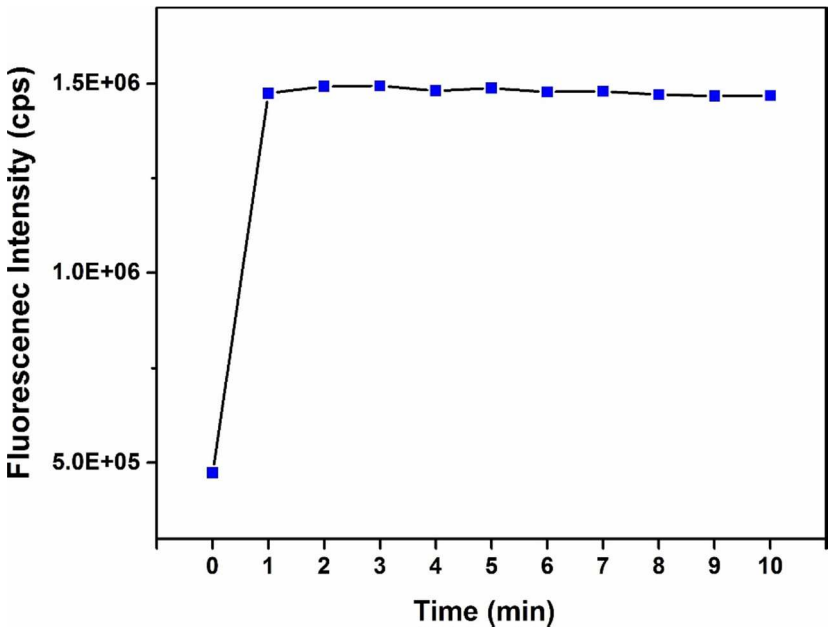

Figure S22. Change in the fluorescence intensity of **1′** in presence of 0.5 mM $ONOO^-$ as a function of time (λ_{ex} = 330 nm and λ_{em} = 426 nm).

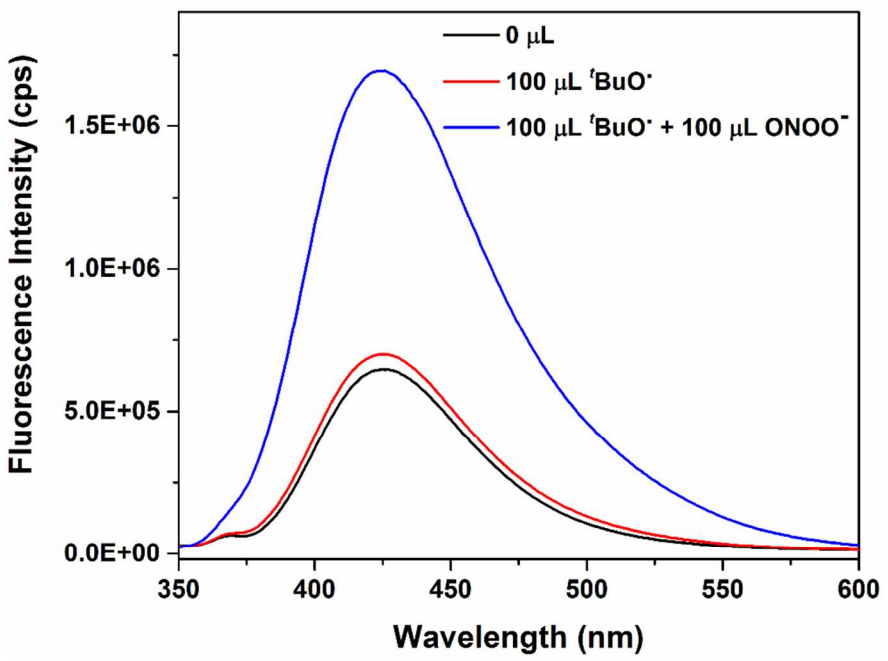

Figure S23. Fluorescence response of **1′** towards 0.5 mM $ONOO^-$ in presence of 0.5 mM $^tBuO^\bullet$ (λ_{ex} = 330 nm and λ_{em} = 426 nm).

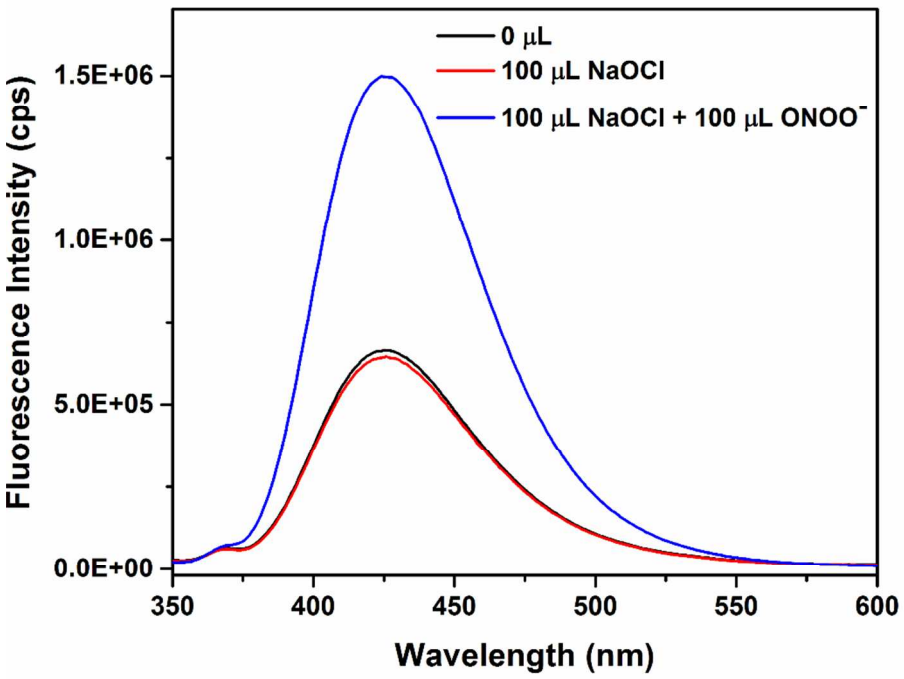

Figure S24. Fluorescence response of **1'** towards 0.5 mM $ONOO^-$ in presence of 0.5 mM NaOCl (λ_{ex} = 330 nm and λ_{em} = 426 nm).

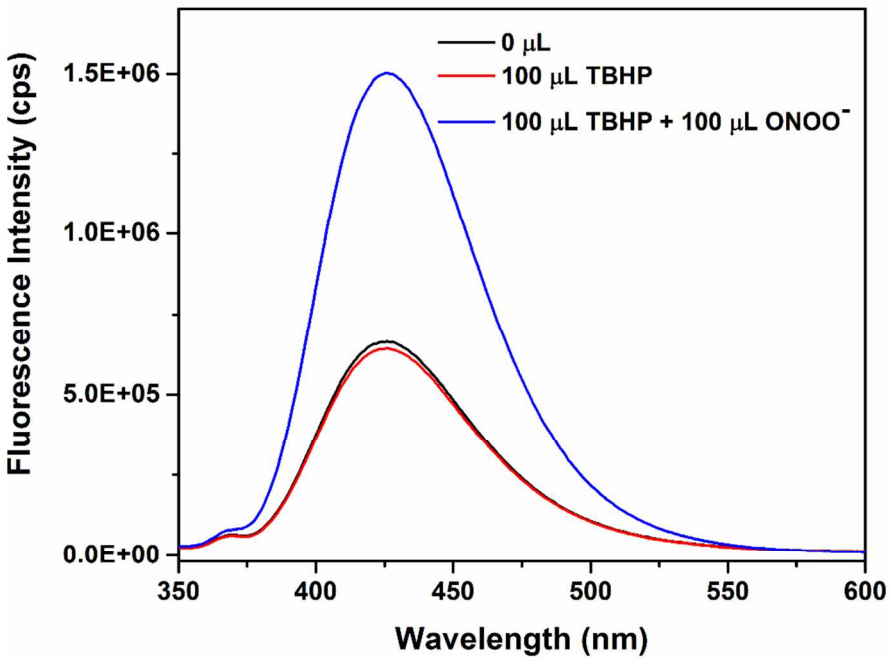

Figure S25. Fluorescence response of **1′** towards 0.5 mM $ONOO^-$ in presence of 0.5 mM TBHP (λ_{ex} = 330 nm and λ_{em} = 426 nm).

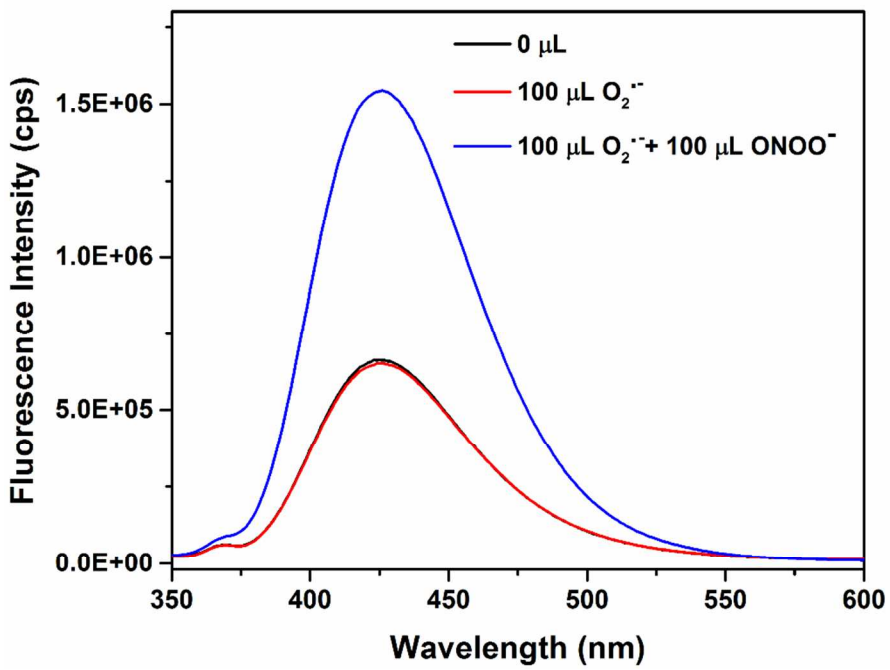

Figure S26. Fluorescence response of **1′** towards 0.5 mM $ONOO^-$ in presence of 0.5 mM $O_2^{\bullet-}$ (λ_{ex} = 330 nm and λ_{em} = 426 nm).

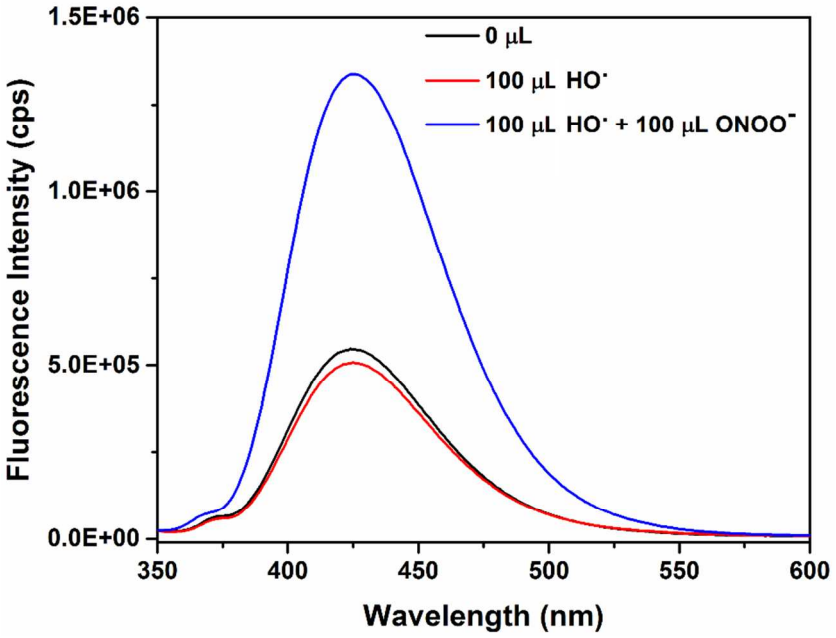

Figure S27. Fluorescence response of **1′** towards 0.5 mM $ONOO^-$ in presence of 0.5 mM $HO^{\bullet}$ (λ_{ex} = 330 nm and λ_{em} = 426 nm).

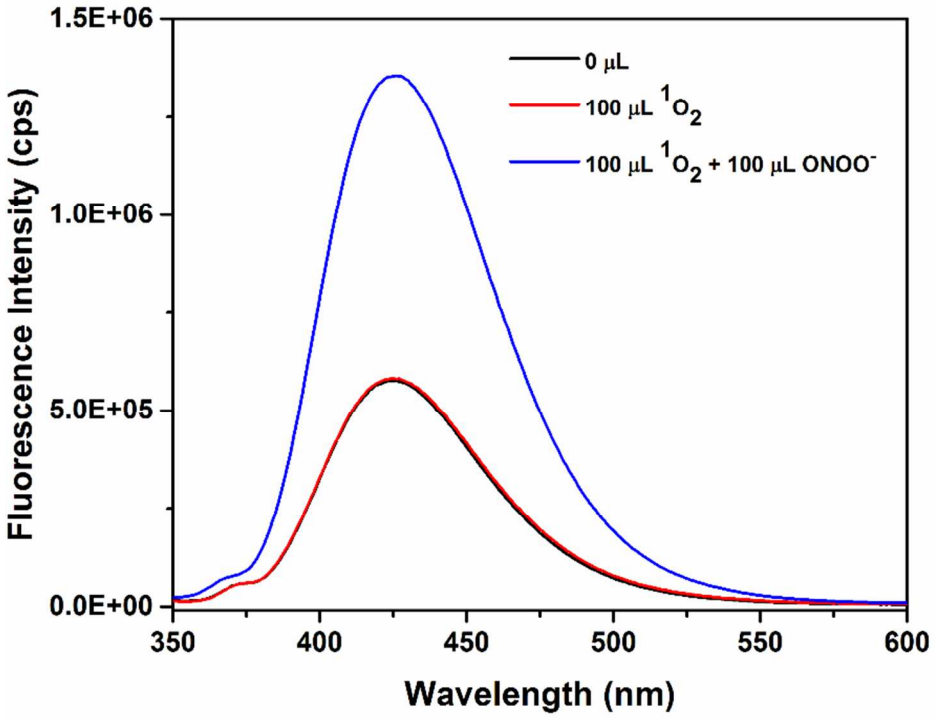

Figure S28. Fluorescence response of **1′** towards 0.5 mM $ONOO^-$ in presence of 0.5 mM $^1O_2$ (λ_{ex} = 330 nm and λ_{em} = 426 nm).

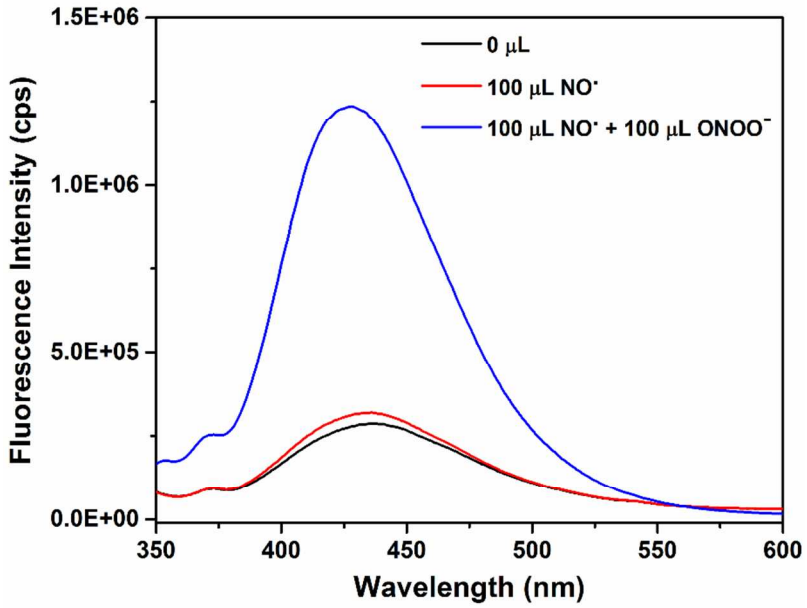

Figure S29. Fluorescence response of **1′** towards 0.5 mM $ONOO^-$ in presence of 0.5 mM $NO^{\bullet}$ (λ_{ex} = 330 nm and λ_{em} = 426 nm).

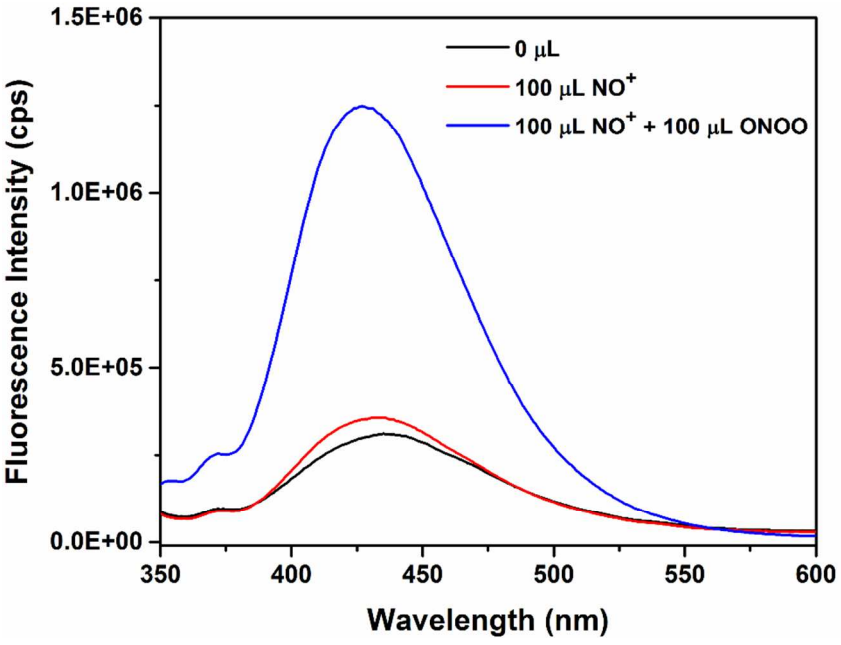

Figure S30. Fluorescence response of **1′** towards 0.5 mM $ONOO^-$ in presence of 0.5 mM NO^+ (λ_{ex} = 330 nm and λ_{em} = 426 nm).

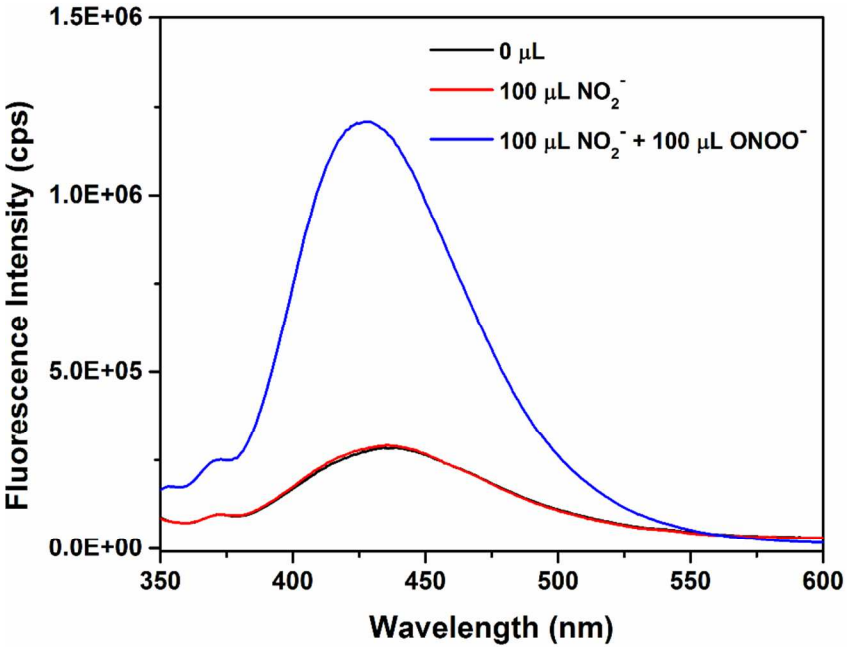

Figure S31. Fluorescence response of **1′** towards 0.5 mM $ONOO^-$ in presence of 0.5 mM NO_2^- (λ_{ex} = 330 nm and λ_{em} = 426 nm).

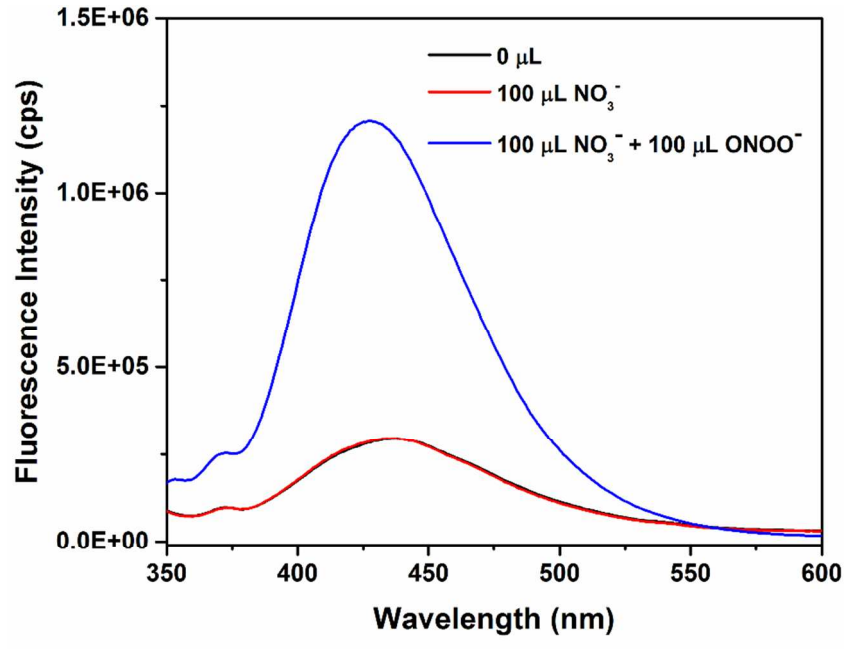

Figure S32. Fluorescence response of **1′** towards 0.5 mM $ONOO^-$ in presence of 0.5 mM NO_3^- (λ_{ex} = 330 nm and λ_{em} = 426 nm).

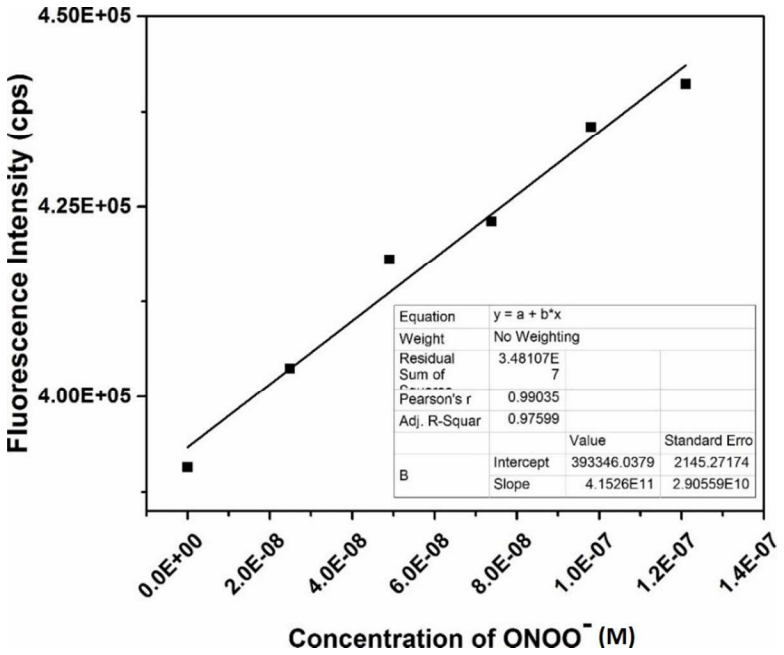

Figure S33. Change in the fluorescence intensity of **1′** in 10 mM HEPES suspension (pH = 7.4) as a function of $ONOO^-$ concentration.

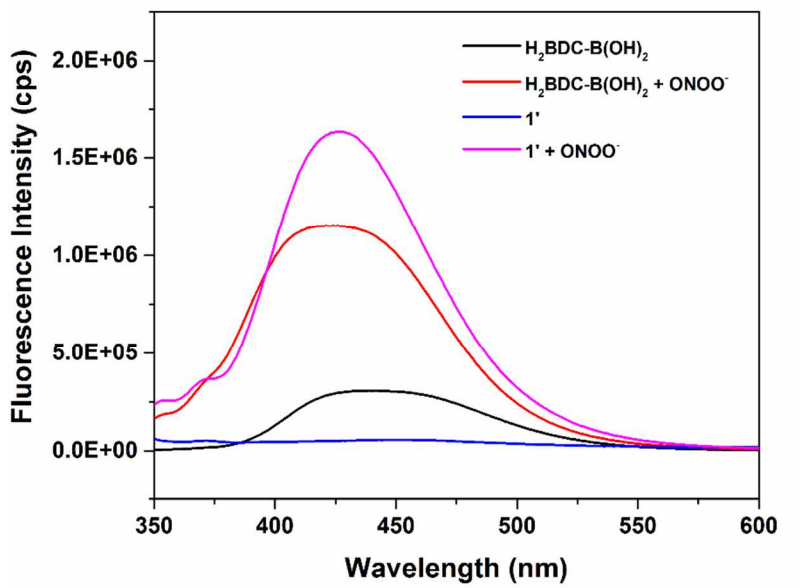

Figure S34. Fluorescence turn-on response of **1′** and free $H_2BDC\text{-}B(OH)_2$ ligand towards the addition of 100 µL peroxynitrite (0.5 mM) in 10 mM HEPES buffer (pH = 7.4).

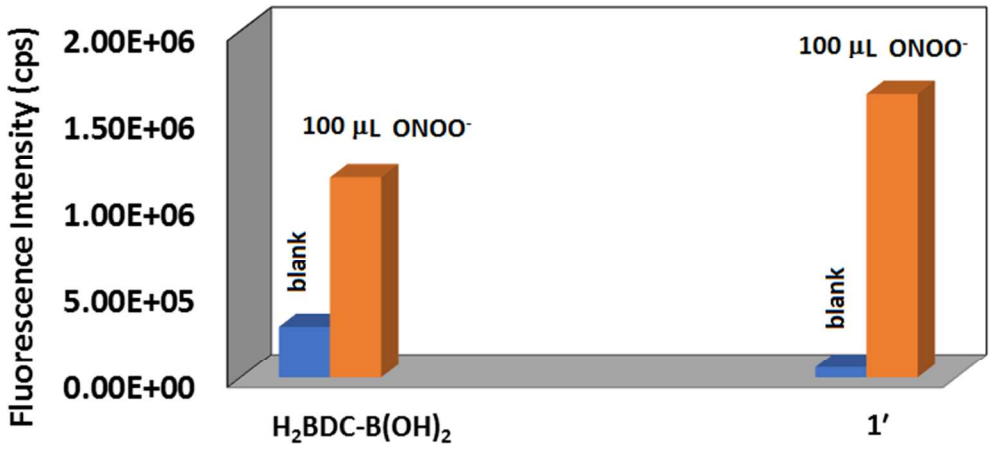

Figure S35. Fluorescence increment behavior of **1′** and free $H_2BDC\text{-}B(OH)_2$ ligand towards the addition of 100 µL peroxynitrite (0.5 mM) in 10 mM HEPES buffer (pH = 7.4).

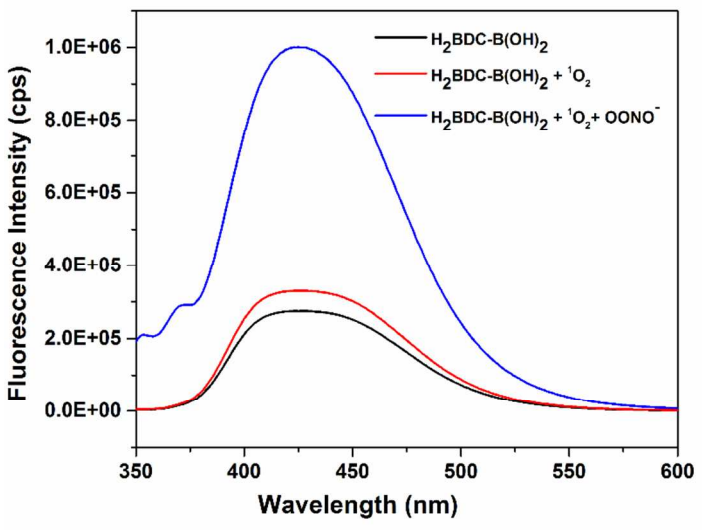

Figure S36. Selective fluorescence turn-on response of the free $H_2BDC\text{-}B(OH)_2$ ligand towards 100 µL peroxynitrite (0.5 mM) in presence of 100 µL of 0.5 mM $^1O_2$ (λ_{ex} = 330 nm and λ_{em} = 426 nm).

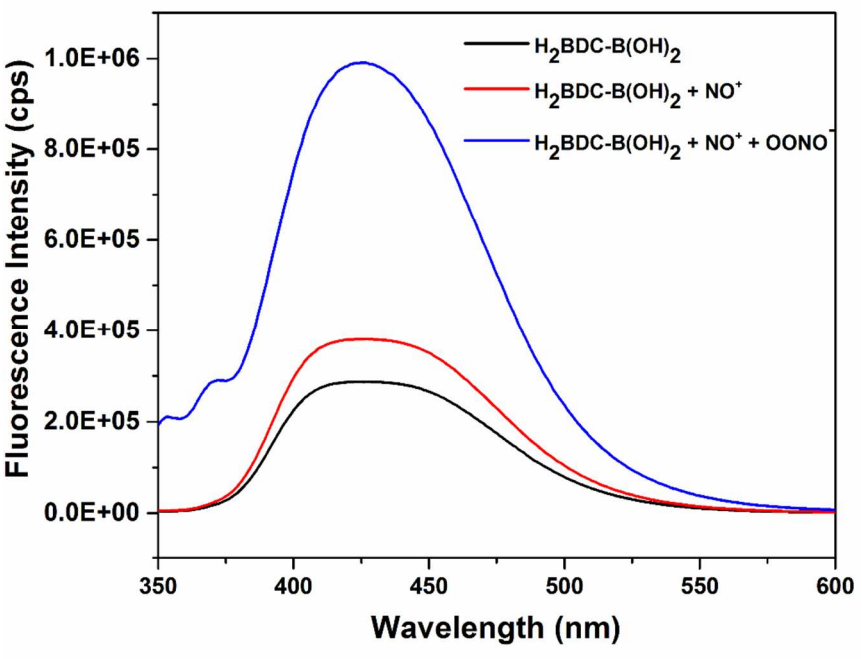

Figure S37. Selective fluorescence turn-on response of the free $H_2BDC\text{-}B(OH)_2$ ligand towards 100 µL peroxynitrite (0.5 mM) in presence of 100 µL of 0.5 mM NO^+ (λ_{ex} = 330 nm and λ_{em} = 426 nm).

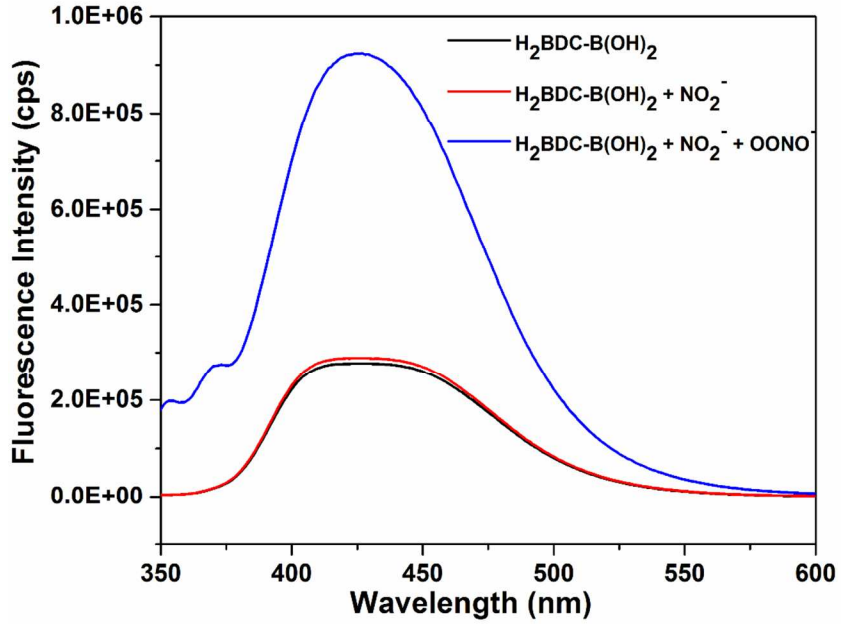

Figure S38. Selective fluorescence turn-on response of the free $H_2BDC\text{-}B(OH)_2$ ligand towards 100 µL peroxynitrite (0.5 mM) in presence of 100 µL of 0.5 mM NO_2^- (λ_{ex} = 330 nm and λ_{em} = 426 nm).

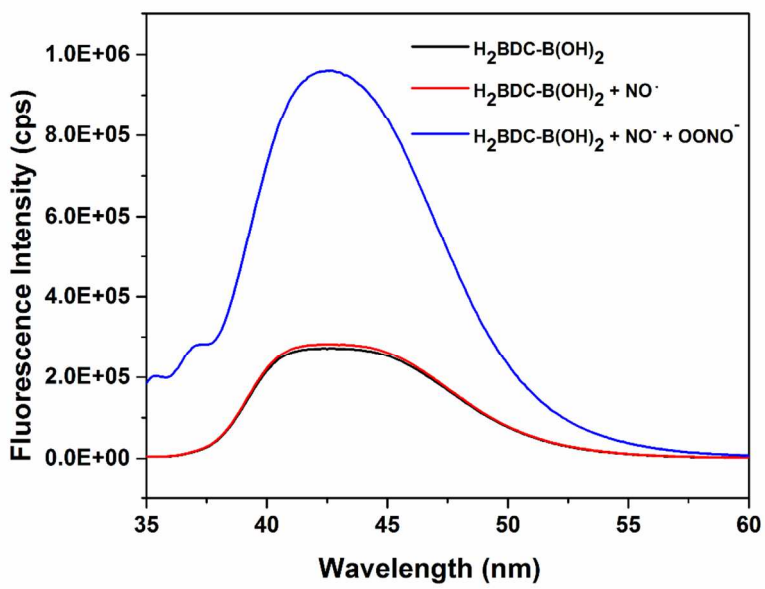

Figure S39. Selective fluorescence turn-on response of the free $H_2BDC\text{-}B(OH)_2$ ligand towards 100 µL peroxynitrite (0.5 mM) in presence of 100 µL of 0.5 mM $NO^{\bullet}$ (λ_{ex} = 330 nm and λ_{em} = 426 nm).

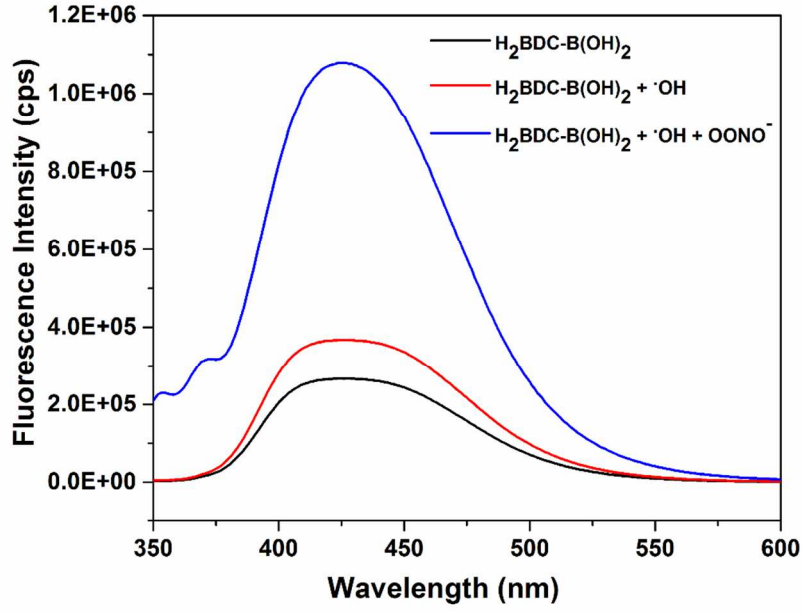

Figure S40. Selective fluorescence turn-on response of the free $H_2BDC\text{-}B(OH)_2$ ligand towards 100 µL peroxynitrite (0.5 mM) in presence of 100 µL of 0.5 mM $HO^{\bullet}$ (λ_{ex} = 330 nm and λ_{em} = 426 nm).

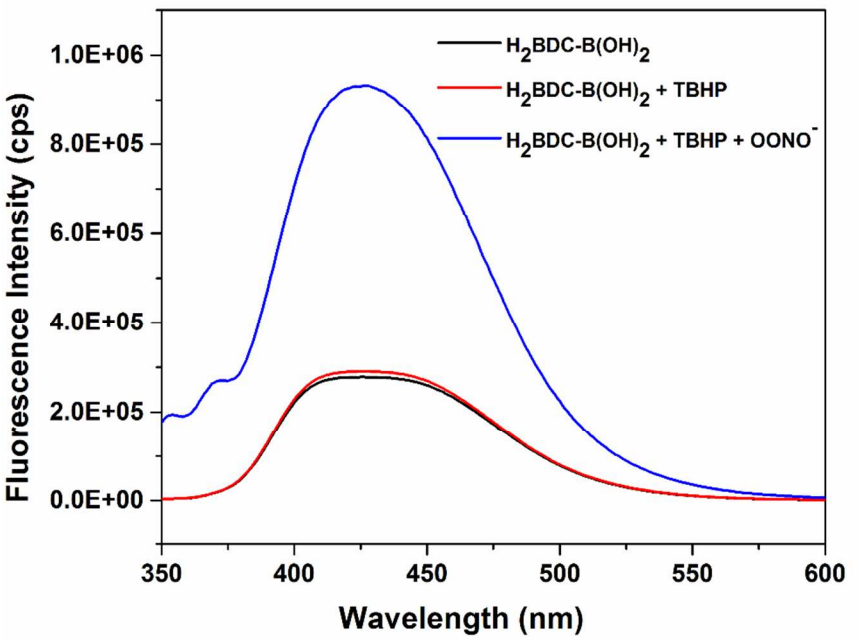

Figure S41. Selective fluorescence turn-on response of the free $H_2BDC\text{-}B(OH)_2$ ligand towards 100 µL peroxynitrite (0.5 mM) in presence of 100 µL of 0.5 mM TBHP (λ_{ex} = 330 nm and λ_{em} = 426 nm).

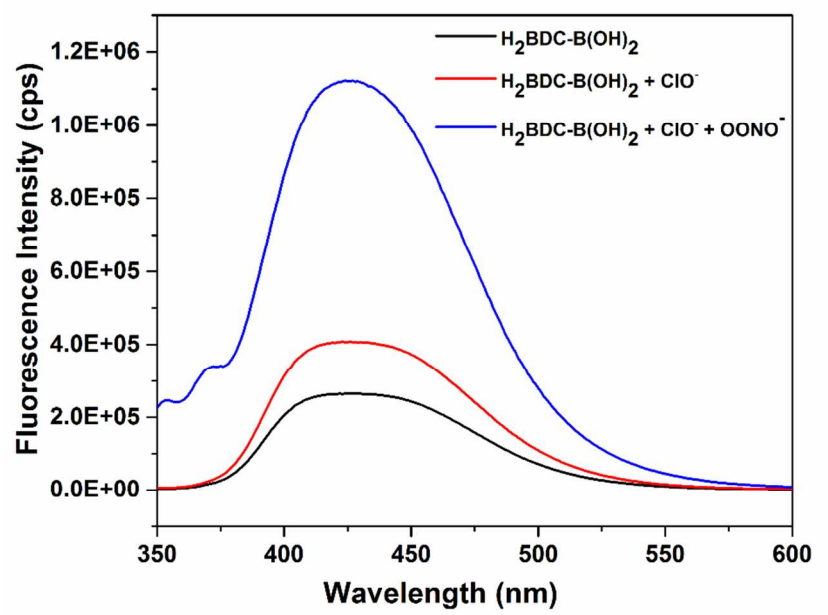

Figure S42. Selective fluorescence turn-on response of the free $H_2BDC\text{-}B(OH)_2$ ligand towards 100 µL peroxynitrite (0.5 mM) in presence of 100 µL of 0.5 mM NaOCl (λ_{ex} = 330 nm and λ_{em} = 426 nm).

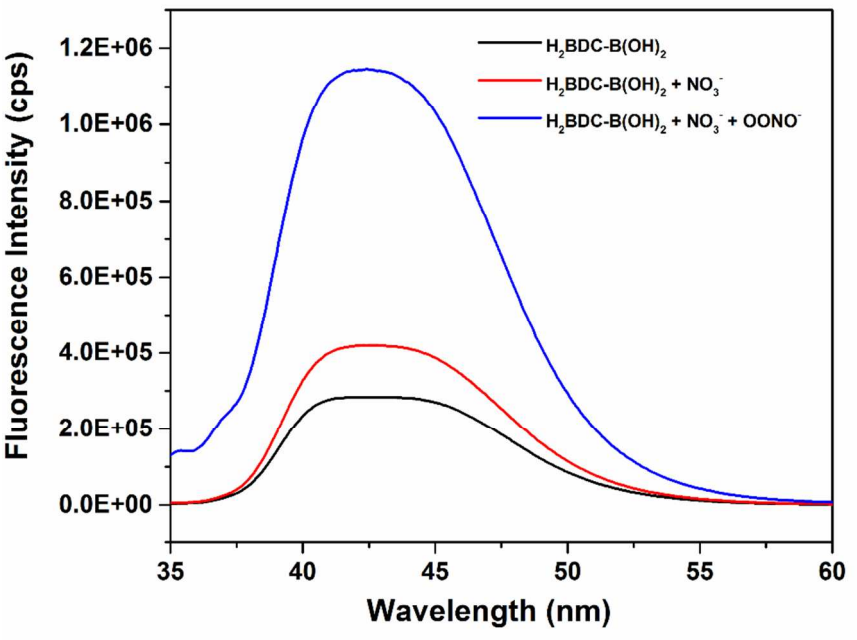

Figure S43. Selective fluorescence turn-on response of the free $H_2BDC\text{-}B(OH)_2$ ligand towards 100 µL peroxynitrite (0.5 mM) in presence of 100 µL of 0.5 mM NO_3^- (λ_{ex} = 330 nm and λ_{em} = 426 nm).

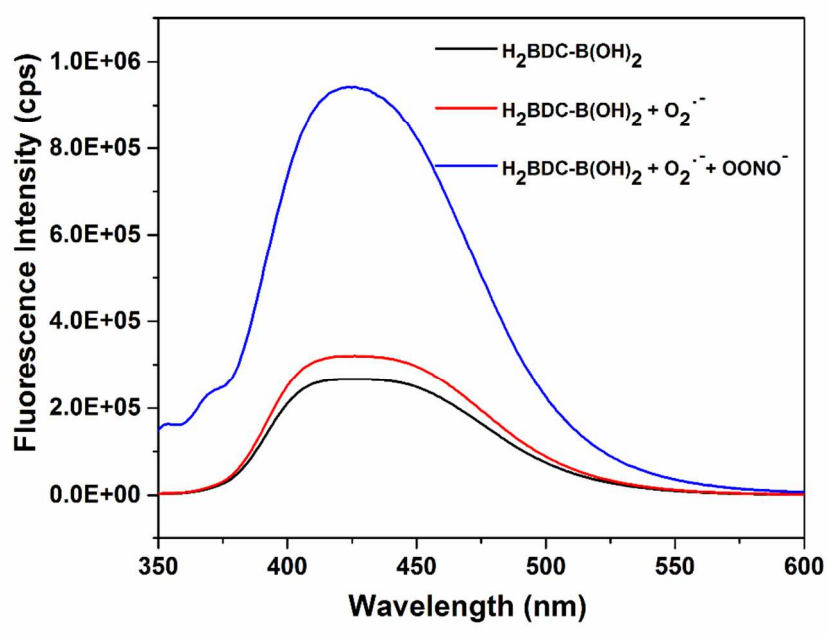

Figure S44. Selective fluorescence turn-on response of the free $H_2BDC\text{-}B(OH)_2$ ligand towards 100 µL peroxynitrite (0.5 mM) in presence of 100 µL of 0.5 mM $O_2^{\bullet-}$ (λ_{ex} = 330 nm and λ_{em} = 426 nm).

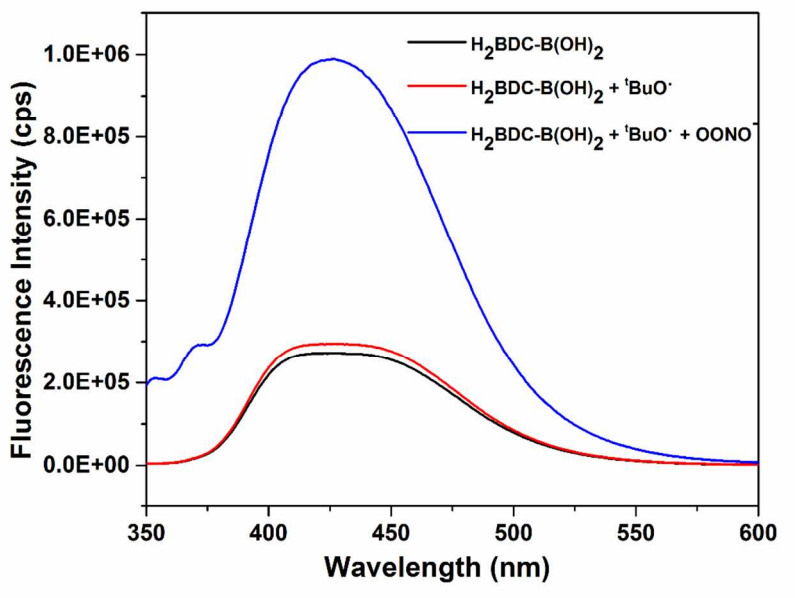

Figure S45. Selective fluorescence turn-on response of the free $H_2BDC\text{-}B(OH)_2$ ligand towards 100 µL peroxynitrite (0.5 mM) in presence of 100 µL of 0.5 mM $^{t}BuO^{\bullet}$ (λ_{ex} = 330 nm and λ_{em} = 426 nm).

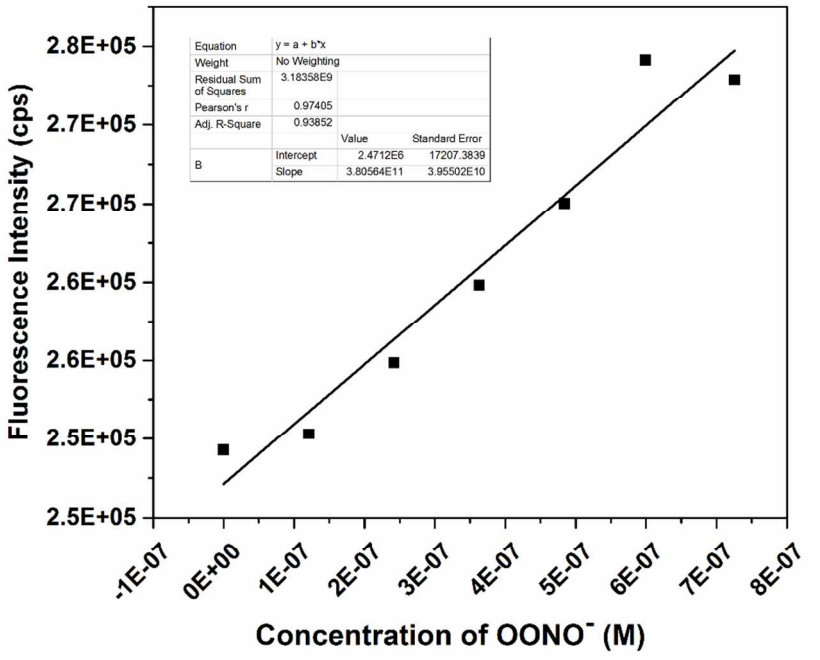

Figure S46. Change in the fluorescence intensity of $H_2BDC\text{-}B(OH)_2$ ligand in 10 mM HEPES buffer (pH = 7.4) as a function of $ONOO^{-}$ concentration.

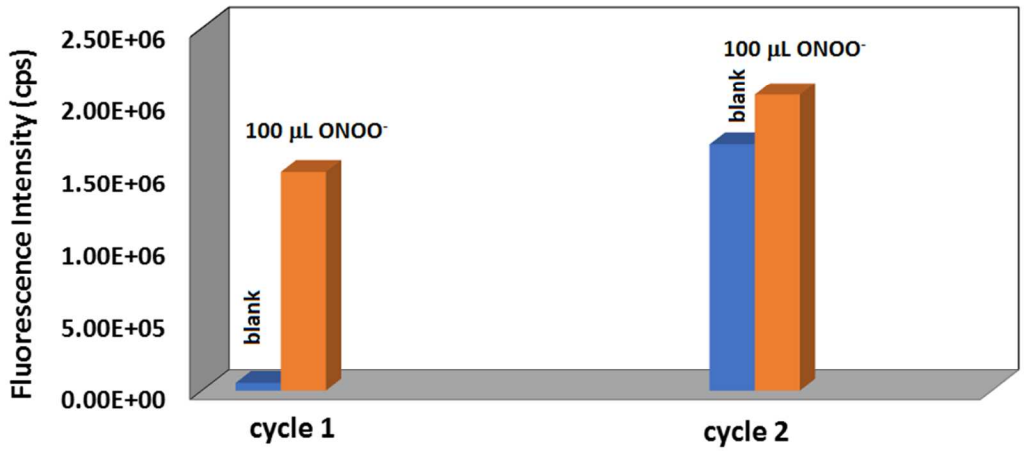

Figure S47. Recyclability test for **1′** towards $ONOO^-$ in HEPES buffer at pH = 7.4 (λ_{ex} = 330 nm and λ_{em} = 426 nm).

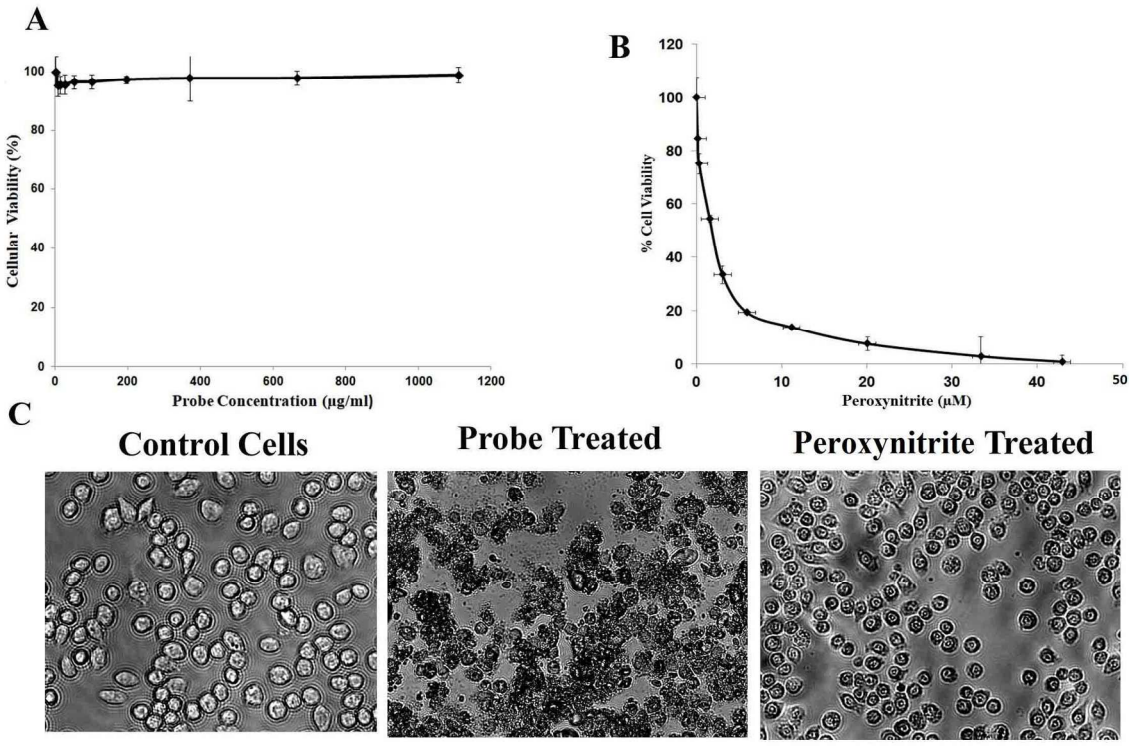

Figure S48. (A) MTT assay for probe-treated macrophage J774A.1cells. (B) MTT assay for peroxynitrite-treated macrophage J774A.1 cells. (C) Morphological analysis of control cells, probe-treated cells and peroxynitrite-treated cells.

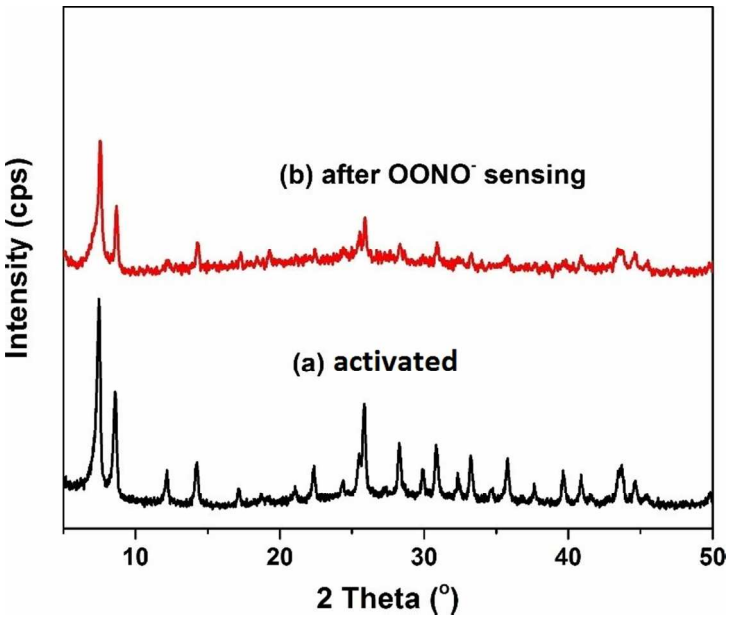

Figure S49. XRPD patterns of **1′** in different forms: activated (a); after peroxynitrite sensing (b).

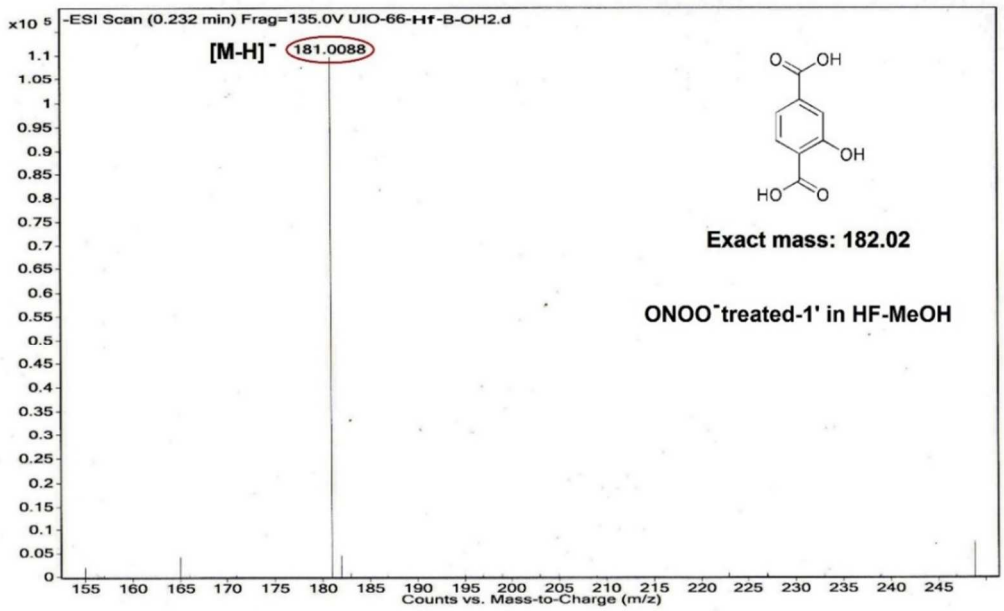

Figure S50. Mass spectrum of **1′** after treatment with $ONOO^-$ in 10 mM HEPES buffer (pH = 7.4).

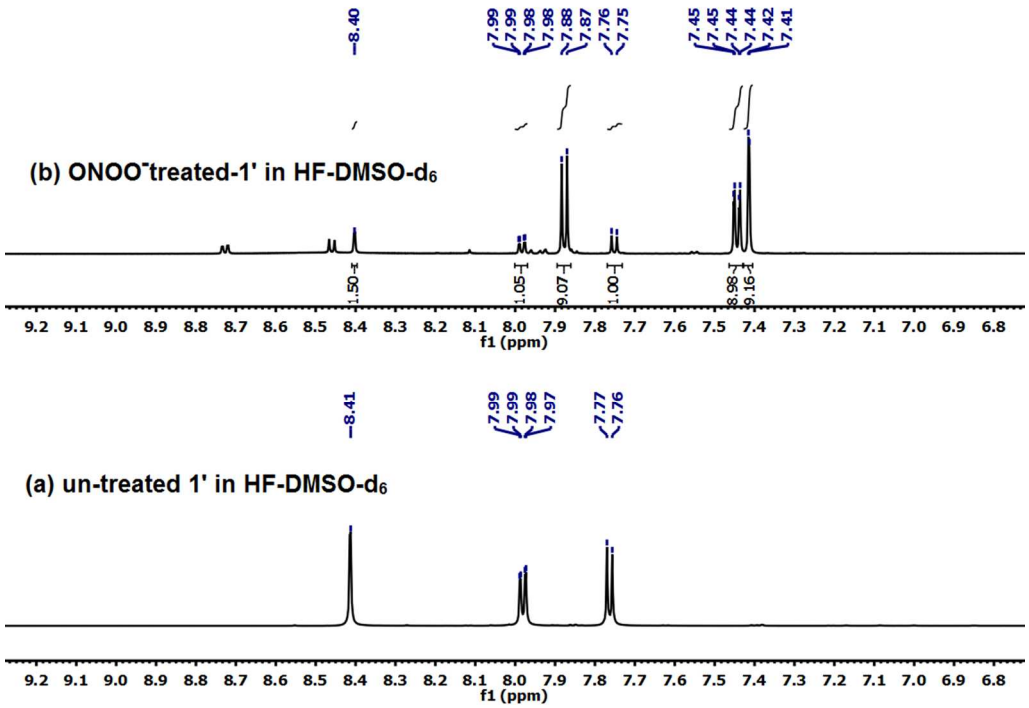

Figure S51. ^{1}H NMR spectra of (a) un-treated **1′** with $ONOO^{-}$ in HF/DMSO-d_6 and (b) $ONOO^{-}$–treated **1′** after digestion in HF/DMSO-d_6.

Table S1. Calculation details for standard deviation (σ) and LOD[#].

Number of Run (n)	Fluorescence Intensities (X) at 426 nm before addition of $ONOO^{-}$	Mean ($\overline{X_i}$)	Standard deviation (σ) = $\sqrt{\frac{\sum(X-\overline{X_i})^2}{n}}$
1.	390748.53	388177.36	1234.09
2.	388246.49		
3.	387333.29		
4.	386855.18		
5.	387051.17		
6.	388256.91		
7.	388749.98		

[#]LOD = $\frac{3\sigma}{K} = \frac{(3\times1234.09)}{(4.15\times10^{11})} = 9.0$ nM

Table S2. Unit cell parameters of the as-synthesized Hf-UiO-66-$B(OH)_2$ MOF. The obtained values were compared with those of the previously reported Hf-UiO-66 MOF.

Compound name	Hf-UiO-66-$B(OH)_2$ (This work)	Hf-UiO-66 (Reported)[1]
Space Group	*Fm-3m* (225)	*Fm-3m* (225)
Crystal System	Cubic	Cubic
a = b = c (Å)	20.733 (8)	20.7006 (3)
α = β= γ (°)	90	90
V ($Å^3$)	8912.3(58)	8870.5(4)
Radiation	Cu $K_{\alpha 1}$	Cu $K_{\alpha 1}$
Figure of Merit (FOM)	16.7	-

Table S3. Comparison of the sensing performance of various peroxynitrite sensors.

A.	Fluorescent sensors						
Sl. No.	Sensor Material	Type of Material	Medium Used	Mode of Sensing	Response Time (s)	Detection Limit	Ref.
1	Hf-UiO-66-$B(OH)_2$	MOF	HEPES buffer	turn-on	60	9.00 nm	This work
2	(i) NMOF-PVA-Abt (MA) (ii) NMOF-PVA-BDY (MB)	MOF	Phosphate buffer	turn-off	(i) 1800 (ii) 600	(i) 0.1 μM (ii) 0.1 μM	2
3	RBPH	Organic molecule	Phosphate buffer	turn-on	180	1.4 nM	3
4	PyBor	Organic molecule	PBS buffer	turn-on	-	0.1 μM	4
5	Fl-B	Organic molecule	Phosphate buffer	turn-on	-	0.25 μM	5

6	RuL	Metal complex	Methanol/ phosphate buffer	turn-off	10	-	6
7	**1**-D-fructose complex	Organic molecule	PBS buffer	turn-off	300	-	7
8	Py-PhB	Organic molecule	DMSO-PBS buffer	turn-on	-	3.54 μM	8
9	HKGreen-1	Organic molecule	Potassium phosphate buffer	turn-on	-	-	9
10	HKGreen-2	Organic molecule	Potassium phosphate buffer	turn-on	2	-	10
11	HKGreen-3	Organic molecule	Phosphate buffer	turn-on		50 nM	11
12	HKGreen-4	Organic molecule	Phosphate buffer	turn-on	-	10 nM	12

B.	Chemiluminescent sensors					
Sl. No.	Sensor Material	Type of Material	Medium Used	Mechanism of Reaction	Incubation Time	Ref.
13	L-012	Organic molecule	Phosphate buffer	Redox	-	13
14	Luminol	Organic molecule	Phosphate buffer	Redox	1800	14
15	PCL-1	Organic molecule	Phosphate buffer	Nucleophilic attack	3600	15

C.	Electrochemical sensors					
Sl. No.	Sensor Material	Type of Material	Mechanism of Reaction	Response Time (s)	Detection Limit	Ref.
16	Pt/Pt black nanoelectrodes	Nanomaterial	Electro-catalytic oxidation	50×10^{-3}	10 fM	16
17	UMS	Electro-polymerised inorganic macromolecular film	Electro-catalytic reduction	-	1.8×10^{-8} mol/L	17
18	Mn-pDPB complex	Conducting polymer	Reduction	15	1.9 nM	18
19	rGO-hemin film on GCE	Hybrid nanomaterial	Electro-catalytic oxidation	20	5 nM	19

20	Nanostructured PEDOT-hemin film	Modified microfibers	Electro-catalytic oxidation	5	200 nM	20
21	Electro-polymerized film of hemin PEDOT	BDD microelectrode	Electro-catalytic oxidation	3.5	10 nM	21
22	rGO/CoPc-COOH on GCE electrode	Modified graphene oxide	Electro-catalytic oxidation	-	1.7 nM	22

References:

1. Jakobsen, S.; Gianolio, D.; Wragg, D. S.; Nilsen, M. H.; Emerich, H.; Silvia, B.; Lamberti, C.; Olsbye, U.; Tilset, M.; Lillerud, K. P. Structural determination of a highly stable metal-organic framework with possible application to interim radioactive waste scavenging: Hf-UiO-66. *Phys. Rev. B* **2012,** 86, 125429-125429.
2. Ding, Z.; Tan, J.; Feng, G.; Yuan, Z.; Wub, C.; Zhang, X. Nanoscale metal–organic frameworks coated with poly(vinyl alcohol) for ratiometric peroxynitrite sensing through FRET. *Chem. Sci.* **2017,** 8, 5101-5106.
3. Ambikapathi, G.; Kempahanumakkagari, S. K.; Lamani, B. R.; Shivanna, D. K.; Maregowda, H. B.; Gupta, A.; Malingappa, P. Bioimaging of peroxynitrite in MCF-7 cells by a new fluorescent probe Rhodamine B phenyl hydrazide. *J. Fluoresc.* **2013,** 23, 705–712.
4. Yu, F.; Song, P.; Li, P.; Wang, B.; Han, K. A fluorescent probe directly detect peroxynitrite based on boronate oxidation and its applications for fluorescence imaging in living cells. *Analyst* **2012,** 137, 3740-3749.
5. Rios, N.; Piacenza, L.; Trujillo, M.; Martínez, A.; Demicheli, V.; Prolo, C.; Álvarez, M. N.; López, G. V.; Radi, R. Sensitive detection and estimation of cell-derived peroxynitrite fluxes using fluorescein-boronate. *Free Radical Biol. Med.* **2016,** 101, 284-295.
6. Ma, J.; Wu, J.; Liu, W.; Wang, P.; Fan, Z. Ruthenium(II) complex-based fluorescent sensor for peroxynitrite. *Spectrochim. Acta, Part A* **2012,** 94, 340-345.
7. Sun, X.; Xu, Q.; Kim, G.; Flower, S. E.; Lowe, J. P.; Yoon, J.; Fossey, J. S.; Qian, X.; Bull, S. D.; James, T. D. A water-soluble boronate-based fluorescent probe for the selective detection of peroxynitrite and imaging in living cells. *Chem. Sci.* **2014,** 5, 3368-3373.
8. Guo, Y.; Lu, G.; Zhuo, J.; Wang, J.; Li, X.; Zhang, Z. A visible-near-infrared fluorescent probe for peroxynitrite with large pseudo-stokes and emission shift via through-bond energy and charge transfers controlled by energy matching. *J. Mater. Chem. B* **2018,** 6, 2489-2496.
9. Yang, D.; Wang, H.-L.; Sun, Z.-N.; Chung, N.-W.; Shen, J.-G. A highly selective fluorescent probe for the detection and imaging of peroxynitrite in living cells. *J. Am. Chem. Soc.* **2006,** 128, 6004-6005.
10. Sun, Z.-N.; Wang, H.-L.; Liu, F.-Q.; Chen, Y.; Kwong, P.; Tam, H.; Yang, D. Bodipy-based fluorescent probe for peroxynitrite detection and imaging in living cells. *Org. Lett.* **2009,** 11, 1887-1890.
11. Peng, T.; Yang, D. HKGreen-3: A rhodol-based fluorescent probe for peroxynitrite. *Org. Lett.* **2010,** 12, 4932-4935.

12. Peng, T.; Wong, N.-K.; Chen, X.; Chan, Y.-K.; Ho, D. H.-H.; Sun, Z.; Shen, J. J. H. J.; El-Nezami, H.; Yang, D. Molecular imaging of peroxynitrite with HKGreen-4 in live cells and tissues. *J. Am. Chem. Soc.* **2014,** 136, 11728−11734.
13. Kielland, A.; Blom, T.; Nandakumar, K. S.; Holmdahl, R.; Blomhoff, R.; Carlsen, H. In vivo imaging of reactive oxygen and nitrogen species in inflammation using the luminescent probe L-012. *Free Radical Biol. Med.* **2009,** 47, 760-766.
14. Alvarez, M. N.; Piacenza, L.; Irigoín, F.; Peluffo, G.; Radi, R. Macrophage-derived peroxynitrite diffusion and toxicity to trypanosoma cruzi. *Arch. Biochem. Biophys.* **2004,** 432, 222-232.
15. Sieracki, N. A.; Gantner, B. N.; Mao, M.; Horner, J. H.; Ye, R. D.; Malik, A. B.; Newcomb, M. E.; Bonini, M. G. Bioluminescent detection of peroxynitrite with a boronic acid-caged luciferin. *Free Radical Biol. Med.* **2013,** 61, 40–50.
16. Wanga, Y.; Noëla, J.-M.; Velmurugana, J.; Nogalaa, W.; Mirkina, M. V.; Lub, C.; Collignonb, M. G.; Lemaîtreb, F.; Amatore, C. Nanoelectrodes for determination of reactive oxygen and nitrogen species inside murine macrophages. *Proc. Natl. Acad. Sci. U. S. A.* **2012,** 109, 11534–11539.
17. Xue, J.; Ying, X.; Chen, J.; Xian, Y.; Jin, L. Amperometric ultramicrosensors for peroxynitrite detection and its application toward single myocardial cells. *Anal. Chem.* **2000,** 72, 5313–5321.
18. Koh, W. C. A.; Son, J. I.; Choe, E. S.; Shim, Y.-B. Electrochemical detection of peroxynitrite using a biosensor based on a conducting polymer−manganese ion complex. *Anal. Chem.* **2010,** 82, 10075–10082.
19. Oprea, R.; Peteu, S. F.; Subramanian, P.; Qi, W.; Pichonat, E.; Happy, H.; Bayachou, M.; Boukherrouba, R.; Szunerits, S. Peroxynitrite activity of hemin-functionalized reduced graphene oxide. *Analyst* **2013,** 138, 4345-4352.
20. Peteu, S. F.; Bose, T.; Bayachou, M. Polymerized hemin as an electrocatalytic platform for peroxynitrite's oxidation and detection. *Anal. Chim. Acta* **2013**, 81-88.
21. Peteu, S. F.; Whitman, B. W.; Galligan, J. J.; Swain, G. M. Electrochemical detection of peroxynitrite using hemin–PEDOT functionalized boron-doped diamond microelectrode. *Analyst* **2016,** 141, 1796-1806.
22. Hosu, I. S.; Wang, Q.; Vasilescu, A.; Peteu, S. F.; Raditoiu, V.; Railian, S.; Zaitsev, V.; Turcheniuk, K.; Wang, Q.; Li, M.; Boukherroub, R.; Szunerits, S. Cobalt phthalocyanine tetracarboxylic acid modified reduced graphene oxide: a sensitive matrix for the electrocatalytic detection of peroxynitrite and hydrogen peroxide. *RSC Adv.* **2015,** 5, 1474-1484.